A Modeling Analysis Program for the JPL Table Mountain Io Sodium Cloud Data

William H. Smyth

Atmospheric and Environmental Research, Inc.
840 Memorial Drive
Cambridge, Massachusetts 02139

and

Bruce A. Goldberg

Jet Propulsion Laboratory
4800 Oak Grove Drive
Pasadena, California

August 1986

Annual Report for Period
June 1, 1985 to May 31, 1986

Prepared for
NASA Headquarters
by AER

TECHNICAL REPORT STANDARD TITLE PAGE

1. Report No.	2. Government Accession No.	3. Recipient's Catalog No.

4. Title and Subtitle	5. Report Date
A Modeling Analysis Program for the JPL Table Mountain Io Sodium Cloud	August 1986
	6. Performing Organization Code
7. Author(s)	8. Performing Organization Report No.
William H. Smyth	
9. Performing Organization Name and Address	10. Work Unit No.
Atmospheric and Environmental Research, Inc. 840 Memorial Drive Cambridge, Ma 02139	11. Contract or Grant No. NASW-3949
	13. Type of Report and Period Covered
12. Sponsoring Agency Name and Address	Annual Report 6/1/85-5/31/86
NASA Headquarters Contracts and Grants Division Washington, DC 20546	14. Sponsoring Agency Code
15. Supplementary Notes	

16. Abstract

Progress and achievements in the second year are discussed in three main areas: (1) data quality review of the 1981 Region B/C images, (2) data processing activities, and (3) modeling activities. The data quality review revealed that almost all 1981 Region B/C images are of sufficient quality to be valuable in the analyses of the JPL data set. In the second area, the major milestone reached was the successful development and application of complex image-processing software required to render the original image data suitable for modeling analysis studies. In the third area, the lifetime description of sodium atoms in the planet magnetosphere was improved in the model to include the offset dipole nature of the magnetic field as well as an east-west electric field. These improvements are important in properly representing the basic morphology as well as the east-west asymmetries of the sodium cloud.

17. Key Words (Selected by Author(s))	18. Distribution Statement
satellite atmospheres planetary magnetospheres	

19. Security Classif. (of this report)	20. Security Classif. (of this page)	21. No. of Pages	22. Price*
Unclassified	Unclassified	29	

*For sale by the Clearinghouse for Federal Scientific and Technical Information, Springfield, Virginia 22151.

TABLE OF CONTENTS

LIST OF FIGURES

LIST OF TABLES

I. Introduction

The goals of this project are to provide physical insight into the local structure of Io's atmosphere, the manner by which gases escape the gravitational well of the satellite and produce neutral clouds in the circumplanetary space, the nature of east-west and possible magnetic longitude asymmetries in the plasma torus, and the stability or variability of both the neutral gas clouds and the plasma torus over a several year time period. These goals are pursued in this AER/JPL collaborative effort by studying and modeling the spatial morphology, intensity, and space-time variability of the Io sodium cloud as preserved in the JPL Table Mountain Io sodium cloud data set, the most complete of the Io sodium cloud data sets currently available. This data set documents the 2-D spatial morphology of the D-line emission intensities of the cloud on the sky plane as a function of both Io geocetric phase angle and the magnetic longitude of Io in the System III coordinate frame over a time period from 1976 to 1981. Highly developed and unique models for the Io sodium cloud at AER provide the key tool for extracting physical insights from this data set.

The complete JPL Io sodium cloud data set is composed of 1974-1979 spectral data, 1981 spectral data, 1976-1979 Region B/C image data, 1981 Region B/C image data, and 1981 Region A image data. The complete data set was reviewed and assessed in the first project year (see the 1985 Annual Report). From this review, both the quality and quantity of data acquired in 1981 were in general much superior to the earlier observations. Because of this fact, the primary emphasis of modeling analysis in this project has been directed toward the 1981 data set and, in particular, to the 1981 Region B/C images. Efforts in the second year have therefore focused primarily on the 1981 Region B/C image data.

Progress in the second project year can be divided into three main areas: (1) data quality review for the 1981 Region B/C images, (2) selection and data processing of a subset of 1981 Region B/C images, and (3) physical enhancement of the Io sodium cloud model in preparation for a third year analysis of the data. A major step in the second area was the successful development and application of software at the Multimission Image Processing Laboratory (MIPL) of JPL to remove distortions present in the brightness

distribution of each image. Because there were significant and unavoidable delays encountered in developing this image software in the past two years, the project was extended for a third year to provide the necessary time to analyze the processed image data. The following more detailed discussion of second year progress is divided into the three main areas noted above.

II. Data Quality Review in the 1981 Region B/C Images

Observational parameters for the 263 Region B/C images of the 1981 JPL data acquired over 14 nights are summarized in numerical form in Table 1 and in graphical form in Figure 1. Prior to this project most of these images had been processed only preliminarily to remove background signals. Images on May 4, 5, 12, 13 and June 4 had undergone further processing to remove the instumental response function and to normalize the image intensity. Because of this, the 110 images (42% of the data set) acquired on May 4, 5, 12 and 13 were chosen and thoroughly reviewed during the first project year. As a result of this review, further refinements in the image processing of these data frames were indentified. The quality of the remaining 153 images is reviewed here as a prerequisite for selection of images in our model-data studies.

The results of this data quality review are summarized in Table 2 and were compiled by manual inspection of photographical products for each image produced prior to this project by the Image Processing Laboratory of JPL. Most images are composed by adding three data frames, where each data frame generally represents an exposure time of approximate ten minutes. Some images are, however, composed of only one or two data frames. The quality of the images is rated in the right hand column of Table 2 and qualifying comments are also indicated. As can be seen, almost all of the images are of sufficient quality to be valuable in our analysis of this data set. Those images selected for more detailed studies will, as noted earlier, undergo further image processing.

Table 1

1981 Region B/C Images: Observing Chronology

Date of Observations	Start Conditions			End Conditions		
	Time (UT)	Io Phase Angle (deg)	Magnetic Longitude of Io† (deg)	Time (UT)	Io Phase Angle (deg)	Magnetic Longitude of Io† (deg)
25 March	7:03	25.2	275.3	8:23	36.5	312.7
5 April	5:18	89.6	365.0	7:40	109.5	70.9
6 April	4:33	287.3	290.7	5:52	298.5	327.3
6 April	6:38	305.1	348.5	7:44	314.4	19.1
28 April	4:21	84.0	200.2	8:50	121.9	324.9
29 April	3:18	279.2	117.5	7:15	312.9	227.1
4 May	3:10	215.4	209.2	9:43	271.4	30.8
5 May	3:17	60.0	159.4	9:25	111.7	330.2
6 May	3:07	262.5	101.4	8:27	307.9	249.5
12 May	3:15	44.5	147.5	8:56	92.4	305.7
13 May	3:20	248.9	96.6	8:51	296.0	249.6
4 June	3:34	47.2	377.3	5:48	66.0	79.5
5 June	3:38	251.7	325.6	4:07	255.8	339.1
5 June	5:27	267.2	16.0	5:55	271.1	29.0
6 June	3:48	95.8	278.0	5:56	113.9	337.3
14 June	3:38	282.7	208.4	5:20	297.1	255.7

†System III (1965)

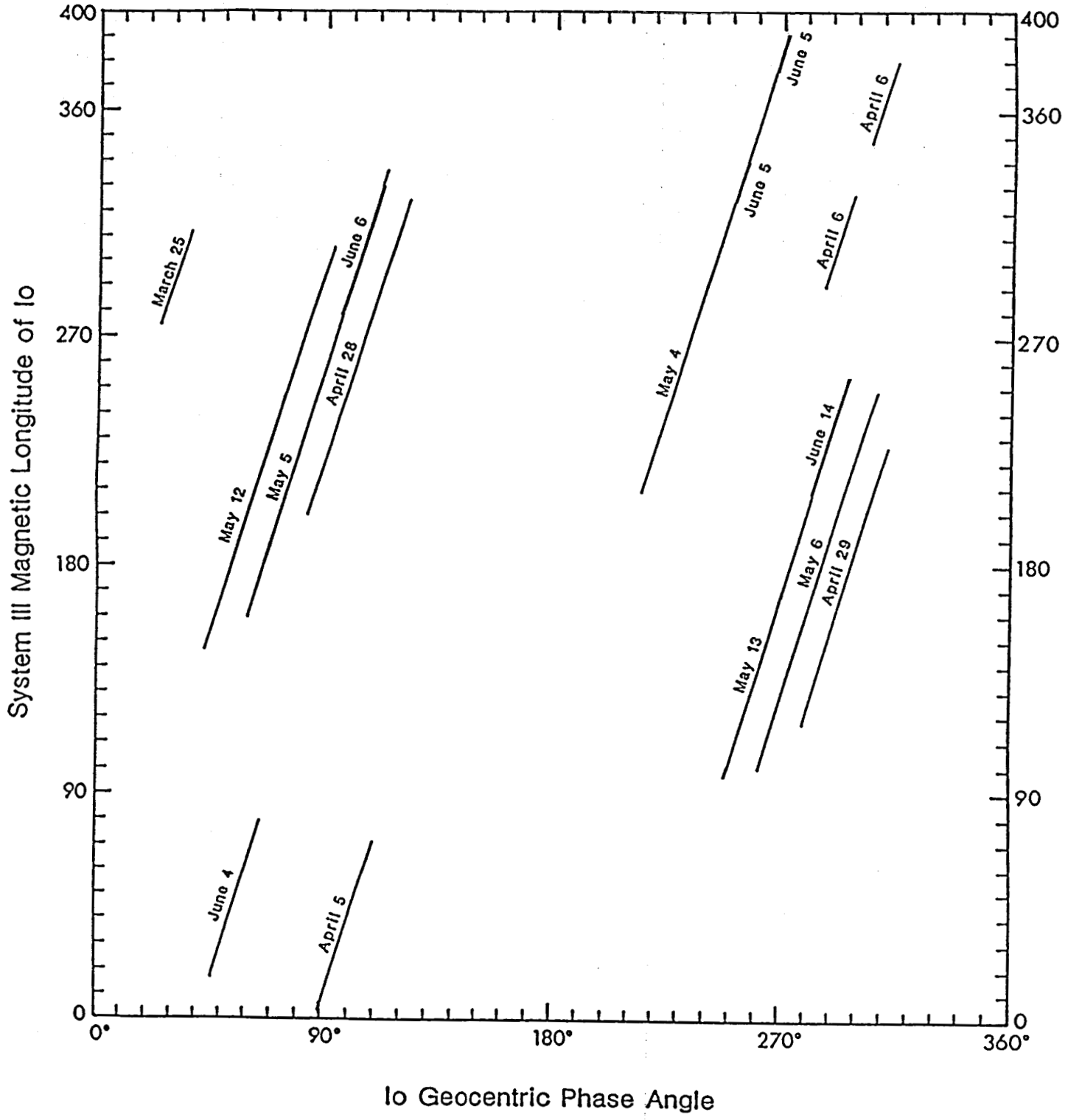

Figure 1. Observing Parameters for 1981 Io Sodium Cloud Images.

The angular coverage for the Io geocentric phase angle and the System III magnetic longitude of Io over which Region B/C images were recorded in the JPL Table Mountain Data Set is indicated for all 14 nights of observations.

Table 2

1981 Region B/C Images: Data Quality Review

Date (UT)	UT Start	UT End	Frames	Quality
March 25	-	-	-	-[1]
	5:11	8:15	29	usable[1]
	-	-	-	-[1]

[1]only raw data available; 16 images with most exposures 1 1/2 minutes, since images were so close to Jupiter; must add images for useful results; images were heavily masked in both east and west directions.

April 5	5:18	5:22	18	marginal[2]
	5:25	5:32	19	good[2]
	5:36	5:46	20	good[2]
	5:48	6:03	21	good[2]
	6:05	6:20	22	good (some saturation)[2]
	6:24	6:44	23	good (some saturation)[2]
	6:47	7:02	24	good[2]
	7:04	7:14	25	very good[2]
	7:17	7:24	26	very good[2]
	7:26	7:36	27	very good[2]
	7:40	7:50	28	very good[2]

[2]Part of forward cloud truncated by mask.

April 6 (one)	4:33	4:40	11	good[3]
	4:42	4:52	12	good[3]
	4:54	5:09	13	good[3]
	5:11	5:28	14	good[3]
	5:30	5:50	15	good[3]
	5:52	6:09	16	good[3]
(two)	6:38	6:55	22	good[3,4]
	6:59	7:09	23	good[3,4]
	7:11	7:23	24	good[3,4]
	7:25	7:42	25	good[3,4]
	7:44	8:01	26	good[3,4]

[3]only raw data available.

[4]probably part of forward cloud truncated.

Table 2

(continued)

Date (UT)	UT Start	UT End	Frames	Quality
April 28	4:21	5:01	25-27	good
	4:37	5:13	26-28	very good
	4:49	5:24	27-29	very good
	5:03	5:34	28-30	very good
	5:15	5:45	29-31	very good
	5:25	5:56	30-32	very good
	5:36	6:07	31-33	very good
	5:47	6:18	32-34	very good
	5:58	6:30	33-35	very good
	6:09	6:40	34-36	excellent
	6:31	6:52	36,38[5]	very good
	6:43	7:03	38,39[6]	very good
	6:54	7:16	39,41[7]	very good
	7:07	7:27	41,42[6]	excellent
	7:07	7:37	41-43	excellent
	7:18	7:46.5	42-44	very good
	7:28	7:57.5	43-45	very good
	7:39	8:07	44-46	very good
	7:49	8:18	45-47	very good
	7:59	8:28	46-48	good
	8:10	8:38	47-49	good
	8:20	8:48	48-50	good
	8:30	8:58	49-51	good

[5]two frames only with 9 minute gap in the middle.

[6]two frames only.

[7]two frames with 1 minute gap in center.

April 29	3:18	3:43	1-3	usable
	3:26	3:57	2-4	good
	3:35	4:07	3-5	good
	3:48	4:19	4-6	good
	3:58	4:32	5-7	very good
	4:10	4:42	6-8	very good
	4:22	4:53	7-9	very good
	4:32	5:05	8-10	very good
	4:44	5:16	9-11	very good[8]
	4:55	5:32	10-12	very good
	5:06	5:43	11-13	very good
	5:21	5:55	12-14	very good[9]
	5:33	6:08	13-15	very good

Table 2

(continued)

Date (UT)	UT Start	UT End	Frames	Quality
April 29 (cont.)	5:45	6:21	14-16	good
	5:57	6:32	15-17	good
	6:10	6:42	16-18	good
	6:23	6:52	17-19	good
	6:33	7:02	18-20	good
	6:43	7:14	19-21	good
	6:53	7:25	20-22	good
May 6	3:07	3:25	5-7	usable (twilight)
	3:12	3:36	6-8	good
	3:18	3:46	7-9	good
	3:27	3:57	8-10	very good
	3:37	4:08	9-11	excellent
	3:47	4:20	10-12	excellent
	3:58	4:32(?)	11-13	excellent
	4:09	4:44	12,13[10]	good
	4:22	5:01	13,15[10]	good
	4:50	5:12	15,16[10]	good
	4:50	5:24	15-17	excellent
	5:03	5:35	16-18	excellent
	5:14	5:47	17-19	excellent
	5:25	5:59	18-20	excellent
	5:36	6:10	19-21	excellent
	5:48	6:20	20-22	excellent
	6:00	6:31	21-23	excellent
	6:11	6:43	22-24	excellent
	6:22	6:54	23-25	excellent
	6:33	7:04	24-26	excellent
	6:44	7:14	25-27	very good
	6:55	7:28	26-28	very good
	7:05	7:40	27-29	very good
	7:18	7:52	28-30	very good
	7:30	8:05	29-31	good
	7:41	8:16	30-32	good
	7:54	8:26	31-33	usable[11]
	-	-	32-34	no good

[8] background level increasing.

[9] little portion of forward cloud truncated by mask.

[10] no signal in frame 14.

[11] Jupiter close to horizon.

Table 2

(continued)

Date (UT)	UT Start	UT End	Frames	Quality
June 4	-	-	-	-[12]
	4:57	5:35	12-14	usable[13]
	5:09	5:47	13-15	usable[13]
	5:24	6:00	14-16	usable[13]
June 5 (one)	3:38	4:05	5-7	marginal[14]
	3:47	4:18	6-8	good[15]
(two)	5:27	6:09	11-13	good[15]
	5:40	6:25	12-14	good
	5:56	6:39	13-15	good
	6:12	6:54	14-16	good
	6:26	7:07	15-17	good
June 6	-	-	-	-[16]
	4:08	4:41	9-11	very good
	4:19	4:53	10-12	very good
	4:30	5:05	11-13	very good
	4:42	5:23	12-14	very good
	4:54	5:42	13-15	very good
	5:08	5:55	14-16	very good
	5:24	6:07	15-17	very good
June 14	3:38	4:04	5-7	usable[17,18]
	3:47	4:15	6-8	good[18]
	3:56	4:28	7-9	good
	4:05	4:40	8-10	good
	4:17	4:52	9-11	good
	4:29	5:05	10-12	good
	4:41	5:19	11-13	good
	4:53	5:32	12-14	good

[12] perhaps more images, but must examine date on tapes.
[13] forward cloud may be partially truncated.
[14] lots of background noise.
[15] some background noise.
[16] possibly more images.
[17] signal to noise not very good
[18] portion of forward cloud truncated by mask

III. Data Processing Activities

1. Data Correlation Studies

Five data correlation studies are defined in Table 3 for the set of 1981 Region B/C images. Each study provides a different classification for these images based upon their Io geocentric phase angle, ϕ, and their Io System III magnetic longitude angle, ψ. The five classifications are useful in identifying and then studying the effects of radiation pressure, the atom source characteristics, and the plasma torus sink characteristics on the morphology of the sodium cloud. Each correlation study lists those images that are appropriate for the defined classification, regardless of the image data-quality summarized in Table 2. Incorporating the results of Table 2 will then aid in selection and prioritization of images to undergo further image processing and then model-data analysis.

The results of the five data correlation studies of Table 3 are summarized in Tables 4-8, respectively. From Table 4, consecutive image studies are possible on all 14 nights, but short exposure times on March 25 and questionable data quality on June 4 might eliminate these two evenings (see Table 2). From Table 5, cloud stability studies are available for three image sequence pairs (also see Figure 1) which all have good to excellent data quality. If comparisons of these image sequence pairs indicate that the sodium cloud and its interaction with the plasma torus are stable over a few month time interval, then the procedure of comparing images of different dates in the correlation studies III, IV and V will represent a valid multi-faceted look at a common (although periodically time dependent) cloud-torus state. From Table 6, east-west image studies of the cloud morphology may be undertaken and used to explore the nature of east-west difference in the plasma torus also identified by optical torus emissions (Morgan and Fertel, 1984; Morgan, 1985) and by UV emission from the Io plasma torus (Sandel and Broadfoot, 1982; Shemansky and Sandel, 1982). From Table 7, System III variations in the electron properties of the plasma torus may be investigated by comparison and analysis of images. From Table 8, the effects of viewing angle on the cloud morphology may be investigated. The effects of system III variation can also be investigated by comparing images for somewhat similar phase angles, and excellent cases exist for ψ in the range from about 160° to 310° (see Table 8 and Figure 1).

Table 3

1981 Region B/C Images: Five Correlation Studies†

I. Consecutive Image Study: $\phi(t)$, $\Psi(t)$

II. Cloud Stability Study: $(\phi_1, \Psi_1) \approx (\phi_2, \Psi_2)$
image sequences separated by 32 days

III. East/West Image Study: $\phi_W = \phi_E + 180°$

$\Psi_E \approx \Psi_W$	only one image-sequence pair
$\Psi_W \approx \Psi_E + 180°$	no image pairs
$\Psi_E \neq \Psi_W$	many comparison images

IV. System III Variability Study: $\phi_1 = \phi_2$, $\Psi_1 \neq \Psi_2$

V. Io Phase Angle Variability Study: $\phi_1 \neq \phi_2$, $\Psi_1 = \Psi_2$

†ϕ = Io Geocentric Phase Angle
Ψ = Io System III Magnetic Longitude Angle

Table 4

1981 Region B/C Images: Correlation Study I

Consecutive Image Study: $\phi(t)$, $\psi(t)$

Image data suitable on all 14 nights

1.	March 25	
2.	April 5	
3.	April 6	
4.	April 28	
5.	April 29	
6.	May 4	(June 5)
7.	May 5	(June 6)
8.	May 6	
9.	May 12	
10.	May 13	(June 14)
11.	June 4	

Table 5

1981 Region B/C Images: Correlation Study II

Cloud Stability Study: $(\phi_1, \psi_1) \approx (\phi_2, \psi_2)$

Three Image Sequence Pairs Suitable

(May 5, June 6)	Io east of Jupiter
(May 4, June 5)	Io west of Jupiter
(May 13, June 14)	Io west of Jupiter

Table 6

1981 Region B/C Images: Correlation Study III

East/West Image Study: $\phi_W = \phi_E + 180°$

1. East Images

ϕ_E	ϕ_W
March 25	May 4
May 12	May 4, May 6, May 13, June 5 (one, two)
June 4	May 4
May 5	April 29, May 4, May 6, May 13, June 5 (one, two)
June 6	April 6 (one), April 29, May 4, May 13, June 14
April 28	April 6 (one)*, April 29, May 4, May 6, May 13, June 5 (two), June 14

2. West Images

ϕ_E	ϕ_W
May 4	March 25, April 5, April 28, May 5, May 12, June 4
June 5 (one)	May 5, May 12
June 5 (two)	April 5, April 28, May 5, May 12
May 13	April 5, April 28, May 5, May 12, June 6
May 6	April 5, April 28, May 5, May 12, June 6
April 6 (one)	April 5, April 28*, May 5, June 6
April 6 (two)	no candidates
June 14	April 5, April 28, May 5, June 6
April 29	April 5, April 28, May 5, June 6

*$\psi_E \approx \psi_W$ in addition

Table 7

1981 Region B/C Images: Correlation Study IV

System III Variability Study†: $\phi_1 = \phi_2$, $\Psi_1 \neq \Psi_2$

Io East of Jupiter			Io West of Jupiter		
ϕ	Date	Ψ	ϕ	Date .. Ψ	
50	June 4	26	250	May 13..102	
	May 12	167		May 4..323	
60	June 4	58	255	May 13..118	
	May 12	198		May 4..338	
				June 5..338	
65	June 4	72			
	May 5	172	260	May 13..133	
	May 12	212		May 4..353	
70	May 5	190	270	June 5...25	
	May 12	231		May 4...25	
				May 6..128	
80	May 5	222		May 13..167	
	May 12	263			
			280	May 6..157	
90	April 5	5		May 13..197	
	April 28	219			
	May 5	256	290	April 29..153	
	May 12	294		May 6..190	
				May 13..232	
100	April 5	37		June 14..232	
	April 28	251		April 6(one)	299
	May 5	288			
	June 6	288	300	April 29..185	
				May 6..223	
110	April 5	70			
	April 28	283	305	April 29..202	
	May 5	322		May 6..238	
	June 6	322		April 6(two)	350
			310	April 6....4	
				April 29..219	

†angles ϕ and ψ given in degrees

Table 8

1981 Region B/C Images: Correlation Study V

Io Phase Angle Variability Study†: $\phi_1 \neq \phi_2$, $\psi_1 = \psi_2$

Ψ	Date	ϕ
0	May 4	262
	April 16(two)	309
10	May 4	265
	April 6(two)	312
20	June 4	48
	April 5	94‡
	May 4	268‡
	June 5(two)	268‡
30	June 4	51
	April 5	97‡
	May 4	271‡
40	June 4	54
	April 5	100
50	June 4	57
	April 5	103
60	June 4	60
	April 5	106
70	June 4	63
	April 5	109
110	May 13	253
	May 6	266
120	May 13	256
	May 6	268
	April 29	280
130	May 13	259
	May 6	271
	April 29	283
140	May 13	262
	May 6	274
	April 29	286
150	May 12	45
	May 13	265
	May 6	277
	April 29	289
160	May 12	48
	May 5	60
	May 13	268
	May 6	280
	April 29	292
170	May 12	51
	May 5	63
	May 13	271
	May 6	283
	April 29	295
180	May 12	54
	May 5	66
	May 13	274
	May 6	286
	April 29	298
190	May 12	57
	May 5	69
	May 13	277
	May 6	289
	April 29	301

Table 8

(continued)

Ψ	Date	ϕ
200	May 12	60
	May 5	72
	May 13	280
	May 6	293
	April 29	304
210	May 12	63
	May 5	75
	April 28	87
	May 4	216
	May 13	283
	June 14	283
	May 6	296
	April 29	307
220	May 12	66
	May 5	78
	April 28	90
	May 4	219
	May 13	286
	June 14	286
	May 6	299
	April 29	310
230	May 12	69
	May 5	81
	April 28	93
	May 4	222
	May 13	289
	June 14	289
	May 6	302
240	May 12	72
	May 5	84
	April 28	96
	May 4	225
	May 13	292
	June 14	292
	May 6	305
250	May 12	75
	May 5	87
	April 28	99
	May 4	228
	June 14	295
260	May 12	78
	May 5	90
	April 28	102
	May 4	231
270	May 12	81
	May 5	94
	April 28	105
	May 4	234
280	March 25	26
	May 12	84
	June 6	96
	May 5	97
	April 28	108
	May 4	237
290	March 25	29
	May 12	87
	June 6	99
	May 5	100
	April 28	111
	May 4	240
300	March 25	32
	May 12	90
	June 6	102
	May 5	103
	April 28	114†
	May 4	243
	April 6(one)	290†

Table 8

(continued)

Ψ	Date	φ
310	March 25	36
	June 6	105
	May 5	106
	April 28	117†
	May 4	246
	April 6(one)	294†
320	June 6	108
	May 5	109
	April 28	120†
	May 4	249
	April 6(one)	297†
330	June 6	111
	May 4	252
	June 5(one)	252
350	May 4	258
	April 6(two)	306

†Angles φ and ψ given in degrees

‡Io phase angles differ by approximately 180°

2. Development of Data Processing Software

Data processing priorities defined for the JPL Table Mountain Io Sodium cloud data are summarized in Table 9. The first and second priorities require development of special software at MIPL.

The development of software for removal of distortion in the D_2 and D_1 image data (item 1 of Table 9) was successfully completed in the third quarter. This completion marked a major milestone for the project and was by far the most difficult task of Table 9. This development had proceeded much slower than initially expected, partly because of its complexity, but primary because of delays at MIPL beyond our control. These delays were caused by two main factors: (1) major changes in the MIPL computer hardware (and corresponding conversion of all of the MIPL image processing software) that occurred in the first year and a half of this project, and (2) difficulties in scheduling time of sufficiently senior MIPL analysts for actual software development. The new image software is quite complex, and its application to image data requires interactive analyst intervention for each image processed.

The development of software to determine the absolute brightness calibration of an image (item 2 of Table 9) was initiated near the end of the third quarter and completed in the beginning of the fourth quarter. The procedure is straight forward and has been thus far restricted to the 1-D slit data which is sufficient for our calibration process.

3. Application of Data Processing Software

The third data processing priority for the JPL Table Mountain Io sodium cloud data in Table 9 is the application of the image and calibration software to images in preparation for modeling analysis. This application began in the fourth quarter at MIPL and was restricted to 1981 Region B/C images data. At the end of the second project year, twenty-two of these image have been completely processed and several additional images are in progress. The twenty-two completed images are identified in Table 10 in terms of their observation date, integration start and end times, and their SIP tape number plus the ID number of each frame that is co-added to produce the image. The start and end values of the geocentric Io phase angle and system III longitude angle of Io are also given in Table 10. The twenty-two images were selected to yield a useful subset of images appropriate for the data correlation studies discussed above. The absolute brightness calibration for each of these images and others currently being processed are expected to be available early in the third project year.

Table 9

Data Processing Priorities

1. Development of Image Processing Software to Remove Distortion in the Brightness Distribution of Images

    a. Implement improved background subtraction techniques for images.

    b. Improve techniques for removal of image distortion near Io produced by continuum light scattered by Io.

2. Development of Software to Determine the Absolute Brightness Calibration of Images

    a. Analyze 1981 1-D slit data on Io's disk and Region A image data to establish an absolute brightness calibration for the 1981 data.

    b. Analyze 1976-79 1-D slit data on Io's disk to establish a brightness calibration for the 1976-79 data.

3. Application of Software to Prepare Images for Modeling Analysis

    a. Using improved techniques in 1 above, remove brightness morphology distortions in a selected subset of images.

    b. Using the information in 2 above, absolutely calibrate this selected subset of images.

Table 10

1981 Region B/C Images: Processed by MIPL

Date of Observations	Start Conditions			End Conditions			Image ID Number (Tape/frames)
	Time (UT)	Io Phase Angle (deg)	Magnetic Longitude of Io† (deg)	Time (UT)	Io Phase Angle (deg)	Magnetic Longitude of Io† (deg)	
28 April	7:39	111.9	292.0	8:07	115.8	305.0	SIP 415/44-46
29 April	3:48	283.5	131.3	4:19	287.9	145.6	SIP 416/4-6
	4:22	288.3	147.0	4:53	292.7	161.4	SIP 416/7-9
4 May	4:20	225.4	241.6	4:53	230.1	256.8	SIP 417/13-15
	4:56	230.5	258.2	5:33	235.8	275.3	SIP 417/16-18
	7:19	250.9	324.3	7:52	255.6	339.5	SIP 417/27-29
	9:06	266.1	13.7	9:50	272.4	34.1	SIP 417/36-39
5 May	3:59	65.9	178.9	4:30	70.3	193.3	SIP 418/10-12
	4:32	70.5	194.2	5:15	76.6	214.2	SIP 418/13-16
	6:34	87.7	250.9	7:10	92.7	267.6	SIP 418/24-26
	8:03	100.2	292.2	8:35	104.7	307.0	SIP 418/31-33
6 May	5:36	283.6	170.4	6:10	288.5	186.1	SIP 419/19-21
	6:11	288.6	186.6	6:43	293.2	201.4	SIP 419/22-24
12 May	5:05	60.0	198.5	6:28	71.6	237.0	SIP 420/15-20
13 May	6:09	273.0	174.7	6:47	278.4	192.3	SIP 421/34-36
	6:49	278.7	193.2	7:23	283.5	208.9	SIP 421/37-39
	7:25	283.8	209.8	7:58	288.5	225.1	SIP 421/40-42
	8:00	288.7	226.0	8:35	293.7	242.2	SIP 421/43-45
	8:25	292.3	237.6	9:00	297.2	253.8	SIP 421/45-47
6 June	4:19	100.2	292.4	4:53	105.0	308.1	SIP 424/10-12
14 June	3:47	284.0	212.6	4:28	289.8	231.5	SIP 425/6-9
	4:17	288.2	226.5	5:07	295.3	294.6	SIP 425/9-12

†System III (1965)

IV. Modeling Activities

1. Improvements for the Io Sodium Cloud Model

The lifetime description of sodium in the planetary magnetosphere has been improved in the second year to include the offset dipole nature of the magnetic field as well as the effects of the east-west electric field (Barbosa and Kivelson 1983; Ip and Goertz 1983). Inclusion of these factors in the lifetime description is important to model properly the morphology of the sodium cloud as discussed below.

The offset magnetic dipole causes the plasma torus center to be offset from the center of Jupiter. This causes the lifetime of sodium at Io's position to have a slight (but true) system III modulation in addition to the system III oscillation caused by the ~7° tilt between the rotating centrifugal plasma plane and the satellite orbit plane. The lifetime variations due to this oscillation were discussed earlier (see third progress report of the first year). The lifetime modulations due to the dipole offset are relatively small compared to the effects produced by the oscillation. These modulations will modify the amount of sodium present in the cloud but not its basic morphology.

The east-west electric field has three major effects on the plasma properties: (1) a geometric shift of the plasma torus center toward the east, (2) a decrease in the electron temperature of a plasma volume element as it moves from west to east of Jupiter, and (3) a decrease in the electron number density of a plasma volume element as it moves from west to east of Jupiter. These three effects provide a significantly longer lifetime for sodium atoms near Io when the satellite is east of Jupiter than when the satellite is west of Jupiter. This east-west asymmetry in the sodium lifetime (because of electron impact ionization) provides a natural explanation for the east-west intensity asymmetry of the sodium cloud that was initially discovered by Bergstralh (1975, 1977) and noted more recently (in a more spatially extended region about Io) in the JPL Table Mountain sodium cloud image data (Goldberg, Garneau and LaVoie 1984).

2. Preparation for Modeling Analysis in the Third Year

In preparation for third year analysis of image data, model calculations have been performed at AER in the third and fourth quarters of this project year to examine the impact of the new lifetime description (discussed above) on the intensity and morphology of the sodium cloud. To describe the model and the nature of the space/time dependent lifetime on the cloud, two companion papers have been undertaken. The first paper entitled "A General Model for Io's Neutral Gas Clouds: Mathematical Description" is a general model-documentation paper. This paper has been completed and is included in the Appendix. The second paper entitled "A General Model for Io's Neutral Gas Cloud: Application to the Sodium Cloud" explicitly applies the general cloud model to the sodium cloud. The model calculations simulate the basic cloud morphology and the character of the east-west orbital and east-west intensity asymmetries for the sodium cloud that have been previously reported in the literature. The second paper is approximately 80% completed and will be finished in the third project year at which time these two companion papers will be jointly submitted for publication. These publications will extend the more recent AER theoretical contributions to the understanding of the Io sodium cloud (Smyth 1979, 1983; Pilcher et al., 1984; Smyth and Combi 1983, 1984, 1985) and provide a solid basis for the third year analysis.

V. References

Barbosa, D.D., and Kivelson, M.G. (1983) Dawn-Dusk Electric Field Asymmetry of the Io Plasma Torus. Geophys, Res. Lett., 10, 210.

Bergstralh, J.T., Matson, D.L., and Johnson, T.V. (1975) Sodium D-Line Emission from Io: Synoptic Observations from Table Mountain Observatory. Ap. J. Lett., 195, 131.

Bergstralh, J.T., Young, J.W., Matson, D.L., and Johnson, T.V. (1977) Sodium D-Line Emission from Io: A Second Year of Synoptic Observation from Table Mountain Observatory. Ap. J. Lett., 211, L51.

Goldberg, B.A., Garneau, G.W., and LaVoie, S.K. (1984) Io's Sodium Cloud. Science, 226, 512.

Ip, W.-H., and Goertz, C.K. (1983) An Interpretation of the Dawn-Dusk Asymmetry of UV Emission from the Io Plasma Torus. Nature, 302, 232.

Pilcher, C.B., Smyth, W.H., Combi, M.R., and Fertel, J.H. (1984) Io's Sodium Directional Features: Direct Evidence for a Magnetospheric-Wind-Driven Gas Escape Mechanism. Ap.J., 287, 427

Smyth, W.H. (1979) Io's Sodium Cloud: Explanation of the East-West Asymmetries. Ap. J., 234, 1148.

Smyth, W.H. (1983) Io's Sodium Cloud: Explanation of the East-West Asymmetries. II. Ap. J., 264, 708.

Smyth, W.H. and Combi, M.R. (1983) Io's Sodium Cloud: A Model for its Interaction with the Plasma Torus. BAAS, 15, 810.

Smyth, W.H. and Combi, M.R. (1984) Understanding the Escape of Material from Io and its Role in the Planetary Magnetosphere. BAAS, 16, 663.

Smyth, W.H. and Combi, M.R. (1985) Correlating East-West Asymmentries in the Jovian Magnetosphere and the Io Sodium Cloud. BAAS, 17, 695.

APPENDIX

A GENERAL MODEL FOR IO'S NEUTRAL GAS CLOUD: MATHEMATICAL DESCRIPTION

A General Model for Io's Neutral Gas Clouds: Mathematical Description

by

W. H. Smyth

M. R. Combi

Atmospheric and Environmental Research, Inc.
840 Memorial Drive, Cambridge, Massachusetts

[PRELIMINARY DRAFT]

ABSTRACT

A general mathematical formalism for calculating the physical properties of any of Io's neutral gas clouds (Na, K, O, S, SO_2) is presented. The dynamical effects of both the gravitational fields of Io and Jupiter and of solar radiation pressure are included in addition to the many complex space and time dependent interactions that occur between the neutral clouds and the plasma torus. Earlier models have not included these complex space and time dependent interactions. The importance of this new model in studying both the plasma conditions prevalent in the inner planetary magnetosphere and the nature of Io's local atmosphere is discussed. A numerical method for evaluating the physical properties of the neutral clouds has been developed and is described. The mathematical formalism and numerical method are applied to a study of the Io sodium cloud in a companion paper in this issue.

1. Introduction

During the past two decades, Io, the innermost of the four Galilean satellites of Jupiter, and its profound influence on the planetary magnetosphere have been one of the most exciting and intensely studied subjects in the solar system. The first evidence that Jupiter and Io constituted a complex interactive system was introduced by Bigg (1964), who discovered that some of the decametric radio emission of Jupiter was directly influenced by the satellite's orbital and magnetic location about the planet. Since then, a large information base has been accumulated from ground-based observations, rocket measurements, earth-orbiting satellites, and four spacecraft encounters with Jupiter: Pioneer 10 (4 December 1973), Pioneer 11 (2 December 1974), Voyager 1 (5 March 1979), and Voyager 2 (9 July 1979).

From ensuing studies of this information base, a picture for the Io-Jupiter system is emerging and slowly coming into focus. Io has a local atmosphere, although it is not well characterized or structurally understood. Io has extended neutral atmospheres or clouds that exist large distances beyond the gravitational grasp of the satellite and fill partial or somewhat incomplete toroidal-shaped volumes around Jupiter. These clouds occupy an overlapping volume with the Io plasma torus - the most dense part of the planetary magnetosphere - and interact with it through collisional processes including ionization and charge exchange reactions. These interactions not only shape the spatial morphology of the clouds but supply heavy ions to the torus and affect the composition, structure, and energy budget of the plasma torus and its extension into the larger magnetosphere. The primary heavy ions that compose the corotating (or nearly corotating) plasma torus are known to be oxygen (O^+, O^{++}) and sulfur (S^+, S^{++}, S^{+++}), although the relative abundances of these ions throughout the torus volume (even for a two-dimensional longitudinally-averaged picture) are still not well established. Io and its local atmosphere also interact with the corotating plasma torus and planetary magnetic field in ways that are yet to be fully understood. Some of these interactions almost certainly provide ions and energy directly to the plasma torus as well as drive escape mechanisms for gases in the local atmosphere.

For purposes of this paper, a brief review of Io's local and extended atmospheres and their relevant interactions with the plasma torus will be given in section 2. This will provide necessary information for understanding the evolution and motivation for developing the new general neutral gas cloud

model presented in sections 3 and 4. A more complete discussion of Io may be found in several excellent review articles (Nash et al. 1986; Brown, Pilcher and Strobel 1983; Fanale et al. 1982, 1977; Kumar and Hunten 1982; Pilcher and Strobel 1982; Brown and Yung 1976). The paper concludes with a brief summary in Section 5. The new model is applied to the sodium cloud in a companion paper (Smyth and Combi 1986) in this issue. In a series of future papers, the new model will also be applied to other neutral clouds of Io (K, O, S, SO_2).

2. Historical Perspective

Our understanding of Io's local atmosphere, although far from complete, has grown steadily since 1964, when Binder and Cruikshank (1964) reported an anomalous brightening of the satellite's surface as it emerged from eclipse. This post-eclipse brightening suggested a dynamic and volatile atmosphere for Io, for which in 1971 an upper limit surface pressure of approximately 10^{-7} bars was deduced by Smith and Smith (1972) from occultation of the star β Scorpii by the satellite. In the summer of 1972, the discovery by Brown (1974) of sodium optical emission from Io's vicinity and the subsequent observations in 1973 by Trafton, Parkinson and Macy (1974) of an extended sodium cloud well beyond the gravitational reach of Io confirmed the presence of a local atmosphere. This discovery also sparked a large number of earth-based observations of the sodium cloud that have continued over the intervening fourteen years. An ionsophere for Io discovered from analyses of Pioneer 10 S-band radio occultation data (Kilore et al. 1974) provided additional information to characterize the satellite's local atmosphere and its possible interactions with the Jovian magnetosphere (Cloutier et al. 1978). A quantum leap forward in understanding Io's local atmosphere was obtained by the Voyager 1 spacecraft's discovery of active volcanic plumes (Morabito et al. 1979) and detection of SO_2 gas ($\sim 10^{-7}$ bars surface pressure) over one of many hot spots on Io (Pearl et al. 1979). Although SO_2 now appears to be the major constituent of the atmosphere (Kumar 1979), the vertical structure, global extent and surface density variations of the atmosphere still remain uncertain even after much theoretical analysis (Kumar 1980, 1982, 1984, 1985; Summers 1984; Matson and Nash 1983). Insightful information for the density of sodium in Io's local atmosphere is to be expected in the near future, however, upon analysis of novel earth-based observations recently presented by Schneider et al. (1985) of absorption signatures at the sodium D-line wavelengths of reflected sunlight from Europa as it was eclipsed by Io.

The discovery of the Io sodium cloud marked the first of four extended atmospheres that have been detected to date for the satellite as summarized in Table 1. The three more recently detected neutral clouds for Io are potassium in 1975 and atomic oxygen in 1980, both from ground-based observations of optical lines, and atomic sulfur in 1981 from rocket-borne instruments measuring ultraviolet emissions. A fifth cloud of neutral SO_2 is expected, because of the presence of a small amount of SO_2^+ ions measured in the plasma

torus (Bagenal and Sullivan 1981; Bagenal 1985), but has not been detected directly. For sodium, more than 1000 observations of its spatial brightness have been made in the last 14 years, with most of the earlier measurements providing only slit-averaged intensity values and most of the more recent measurements providing increasingly higher-quality two-dimensional image data. For the dimmer potassium cloud (~ 1/20 the brightness of the sodium cloud), about 200 slit-averaged observations have been made almost entirely by Trafton (1975, 1981), who presented a survey of this gas cloud that exhibited spatial and temporal variations similar to those documented for the Io sodium cloud. For the much dimmer atomic oxygen and atomic sulfur clouds, only a very few slit-averaged detection observations have been acquired.

The presence of neutral clouds for Io provides a largely unexplored but rich potential for studying both the plasma conditions prevalent in the inner planetary magnetosphere and the nature of Io's local atmosphere. Sodium is by far the best neutral cloud to use as a probe for these purposes, because it is the brightest and most extensively observed and is (together with potassium) sensitive to spatial and temporal changes in the plasma torus due to its small electron impact ionization lifetime (~ 1-2 hours) near Io's orbit. Early observations acquired in 1973 and 1974 (i.e., pre- and post-Pioneer 10) by Macy and Trafton (1975 a,b) and Münch and Bergstralh (1977), for example, first suggested the presence of a magnetospheric sink for sodium near Io's orbit that was both radially asymmetric and oscillatory. The radial asymmetry was suggested by the presence of a predominatly forward sodium cloud, and the oscillatory nature was suggested by time dependent changes in the sodium brightness north and south of the satellite that were correlated with the satellite's magnetic latitude (Trafton and Macy 1975; Trafton 1980). As will be shown in the companion paper in this issue, the predominantly forward cloud is indeed naturally produced by the radial asymmetry of the plasma torus for sodium ejected from Io at relatively slow speeds (~ 3 km sec^{-1}) as first suggested from these early observations. These slow speed atoms may be energized by magnetospheric ions both directly through scattering of neutrals from the local atmosphere (or surface, if regions of low density exist) as discussed in a number of papers (Sieveka and Johnson 1984; Cheng 1984; Lanzerotti and Brown 1983; Brown, Pilcher and Strobel 1983; Ip 1982; Matson, Johnson and Fanale 1974), and indirectly through multicollisional processes resulting in atmospheric sputtering (Summers, Yung and Haff 1983; Haff, Watson and Yung 1981;

McGrath and Johnson 1986) or blowoff (Hunten 1985). More recent observations of the sodium cloud have shown, for example, (1) well-defined spatial zones that become temporally deficient of atoms, due perhaps to locally (likely System III) enhanced ionization (Goldberg, Garneau, and LaVoie 1984), (2) directional features produced by high-velocity ($\sim$ 20 km sec^{-1}) sodium driven elastically by the magnetospheric wind from the local atmosphere at near right angles to Io's orbit and preferentially from the equatorial regions (Pilcher et al. 1984), and (3) very fast ($\lesssim$ 60 km sec^{-1}) narrowly-collimated jets of sodium driven directly ahead of the satellite by charge exchange reactions with the plasma torus (Trauger 1984, 1985). Although the oxygen and sulfur clouds are only bright enough to be barely detected, physical insight acquired for the bright sodium cloud may be adopted where appropriate in OI, SI and SO_2 cloud models. These atomic and molecular cloud models so constructued then become enhanced tools themselves to determine ion loading rates, plasma mass loading rates, and ion energy input rates to the plasma torus as well as to specify the character and source rate of neutral gases escaping from Io's local atmosphere (Smyth and Shemansky 1983).

Models for the neutral clouds of Io are essential in probing and recovering physical information from spatial brightness observations of Io's extended atmospheres and relating this information to conditions in Io's local atmosphere and the planetary magnetosphere. The development of cloud models for Io was historically initiated for the sodium cloud in the early 1970's and has evolved during the last decade with progressively more complete descriptions for the source, lifetime, and orbital dynamics of sodium atoms in the Jupiter system. Only in the last few years have models for the Io oxygen and sulfur clouds (Smyth and Shemansky 1983) and the Io potassium cloud (Smyth and Combi 1984) been developed. A general model, appropriate to any of these neutral gas clouds of Io, has now been formulated and is presented in Sections 3 and 4.

3. Mathematical Description for the Io Neutral Gas Clouds

Mathematical Approach

The basic mathematical approach is based upon the conservation in phase space of the one-particle distribution function $f(\vec{v},\vec{x},t)$ for a gas species. In brief, if at an initial time $t = t_b$ the distribution function can be specified, then the distribution function at a later time may, under certain circumstances of interest here, be simply related to its initial value by properly mapping its time evolution in phase space and including processes that modify its initial value during this time evolution. This conservation in phase space follows directly from the well-known Liouville's theorem for an N-particle system upon integrating over the six phase-space coordinates of N-1 of these particles.

The general approach may be formally understood as follows. The one-particle distribution function in kinetic theory has the physical meaning that

$$f(\vec{v},\vec{x},t)\, d\vec{x}\, d\vec{v} \tag{1}$$

represents the (ensemble-average) number of atoms (or molecules) at time t in a spatial volume element $d\vec{x}$ about position $\vec{x}$, with velocities $d\vec{v}$ about $\vec{v}$. The time evolution of the one-particle distribution function is governed by the kinetic equation

$$\frac{\partial f}{\partial t} + \vec{v} \cdot \frac{\partial f}{\partial \vec{x}} + \frac{\vec{F}}{m} \cdot \frac{\partial f}{\partial \vec{v}} = \left(\frac{\delta f}{\delta t}\right) \tag{2}$$

where $\vec{F}$, which may in general depend on $(\vec{v},\vec{x},t)$, is the force experienced by the gas atoms (or molecules) due to macroscopic internal and external sources and m is the mass of a gas atom (or molecule). Furthermore, $(\delta f/\delta t)$ is the local rate of change of $f(\vec{v},\vec{x},t)$ due to processes such as collisions that may add or remove the (ensemble-average) number of atoms (or molecules) from an element of phase space. For binary collisions in a gas, for example, one obtains the Boltzmann equation when the right-hand side of the kinetic equation is represented by the Boltzmann collision integral (a nonlinear and integral function of the distribution function).

The time evolution or trajectory of a point in phase space $(\vec{v},\vec{x}) = (\vec{v}(t),\vec{x}(t))$ that is initially $(t=t_b)$ at a point $(\vec{v}_b,\vec{x}_b) = (\vec{v}(t_b),\vec{x}(t_b))$ is

determined by solving the equations of motion for a gas atom (or molecule) of mass m

$$\vec{v}(t) = \frac{d\vec{x}(t)}{dt} \tag{3.a}$$

$$\frac{\vec{F}(\vec{v}(t),\vec{x}(t),t)}{m} = \frac{d\vec{v}(t)}{dt} \tag{3.b}$$

for this initial value problem. These equations of motion are by construction the characteristic equations of the kinetic equation so that the left-hand side of the kinetic equation is the total time derivative of the distribution function. The kinetic equation thus reduces to

$$\frac{df}{dt} = \left(\frac{\delta f}{\delta t}\right) . \tag{4}$$

There exists a class of physical problems to which the Io gas clouds may be related in which the gas density is sufficiently low that gas atoms (or molecules) along their phase space trajectories do not collide with each other but may collisionally interact with other material (such as ions and electrons in a rarefied plasma) or photons (i.e., photoionization or photodissociation processes) so as to change the initial ensemble-average number of atoms. In this case, the right-hand side of the kinetic equation is linear in the distribution function and may be expressed in the general form

$$\left(\frac{\delta f}{\delta t}\right) = -\nu f + S , \tag{5}$$

where ν and S are independent of f but may depend in general upon $(\vec{v},\vec{x},t)$. Here ν is an effective loss rate and S is an effective source rate for the ensemble-average number of atoms in an element of phase space. Using expression (5) in (4), the kinetic equation can be explicitly integrated along the phase space trajectory to determine the distribution function at time t:

$$\begin{aligned} f(\vec{v}(t),\vec{x}(t),t) = {} & f(\vec{v}_b,\vec{x}_b,t_b)\ P(t,t_b) \\ & + \int_{t_b}^{t} dt'\ S(\vec{v}(t'),\vec{x}(t'),t')\ P(t,t') . \end{aligned} \tag{6}$$

Here

$$P(t_2,t_1) = \exp\left[-\int_{t_1}^{t_2} dt'\ \nu(\vec{v}(t'),\vec{x}(t'),t')\right] \tag{7}$$

is the probability that an ensemble-averaged number of gas atoms introduced at a time t_1 exist at a later time t_2 because of the effective loss rate ν. The distribution function at a time $t > t_b$ is then given by the initial distribution function reduced by this probability plus all new source contributions to the initial distribution function that have occurred in the time interval t_b to t with a proper decay loss included for these contributions.

The description of the gas may therefore be constructed in terms of a large number of phase space trajectories along which the ensemble-averaged number of atoms evolve in time based upon a set of initial conditions for the distribution function which properly simulate the boundary conditions of a particular physical problem. More specifically, the description of the gas can be fundamentally reduced to describing the time evolution of an ensemble packet of gas along its phase space trajectory. An ensemble packet is defined as the infinitesimal volume element containing the ensemble-average number of atoms that initially began its trip along the trajectory in the time interval t_b to $t_b + dt$. The physics of an ensemble packet appropriate for the Io neutral gas clouds is described in the next subsection.

The basic principle of the general mathematical approach described above has been employed in planetary science to develop models for a number of studies involving collisionless or nearly collisionless atmospheres. The basic principle has been, in fact, used with increasing regularity in the last two decades. These studies have included cometary atmospheres, planetary atmospheres, and satellite atmospheres for which major references are given in Table 2. A more general review of exospheric theories is given by Fahr and Shizgal (1983). The studies for Io's neutral gas clouds are perhaps the most complex subset of these exospheric problems appropriate to the linear interaction (5). This complexity results because of the inherent velocity, space, and time dependence of <u>both</u> the force $\vec{F}$ in the equations of motion and the effective loss rate ν of neutrals in the plasma torus and also because of the form of the source term S which is described below.

For the Io neutral gas cloud, the source term S in (5) is a spatially distributed source that describes the creation of secondary cloud atoms

produced by interactions of the magnetospheric plasma with only the primary gas cloud atoms (or molecules) initially ejected from the satellite. For atomic gas clouds, the distributed source is caused primarily by charge exchange reactions between the extended cloud atoms and the corotating plasma torus ions. Elastic collisions between these ions and extended cloud atoms may also produce a contribution to the source term in (5) but this contribution is usually significantly less important over the relative short lifetime of the cloud. Primary cloud atoms have velocities relative to Io that are generally slow compared to the corotational ion speed ($\sim$ 57 km sec $^{-1}$) and, when removed by the atom-ion charge exchange reactions, create fast secondary cloud atoms that have a rather tightly confined velocity dispersion centered on the corotational speed. The fast secondary cloud atoms are thus created in a velocity volume of phase space that is generally discontinuous with velocity volume of phase space containing the slow primary cloud atoms. For molecular gas clouds (e.g., SO_2 or SO), electron-impact dissociative reactions very rapidly remove the primary cloud molecules (Shemansky 1984) and create other secondary cloud atoms (or molecules) that initially may have additional amounts of kinetic energy as dictated by the energetics of the reaction. Because of the rapid dissociative lifetime of molecules in the plasma torus, these dissociative sources are likely to be heavily confined near Io. A gas cloud of Io for the j neutral species may therefore be generally described by a primary and a secondary population of cloud atoms (or molecules) by formally dividing the one-particle distribution function (1) into two parts.

$$f_j = f_j^{(\text{primary})} + f_j^{(\text{secondary})} . \tag{8}$$

The kinetic equation (4) with the right hand side given by (5) may thus be formally subdivided for the j species into equations for the primary and secondary atom (or molecule) populations

$$\frac{df_j^{(\text{primary})}}{dt} = -\nu f_j^{(\text{primary})} \tag{9.a}$$

$$\frac{df_j^{(\text{secondary})}}{dt} = -\nu f_j^{(\text{secondary})} + S_j \tag{9.b}$$

where the secondary source term may be written in the form

$$S_j = \sum_k C_{jk} f_k^{(primary)} , \qquad (9.c)$$

where C_{jk} describes the creation rate of secondary cloud atoms (or molecules) of the j species from primary cloud atoms (or molecules) of the k species. The source term (9.c) therefore represents the secondary cloud atoms (or molecules) produced by all primary cloud atoms (or molecules). More generally, a source term similar to (9.c) may likewise be introduced if necessary to include third generation extended source terms produced by dissociation of secondary cloud molecules (e.g. SO → S + O). Limiting the present development to second generation source terms, the description of a neutral cloud is then obtained by first solving (9.a) for the properties of the primary cloud atom (or molecule) population

$$f_j^{(primary)}(v(t),x(t),t) = f_j^{(primary)}(\vec{v}_b,\vec{x}_b,t_b)\, P_j(t,t_b) \qquad (10.a)$$

and then by secondly determining S_j and solving (9.b) for the properties of the secondary cloud atom (or molecule) population

$$f_j^{(secondary)}(\vec{v}(t),\vec{x}(t),t) = \int_{t_s}^{t} dt''\, S_j(\vec{v}(t''),\vec{x}(t''),t'')P_j(t,t'') . \qquad (10.b)$$

where $f_j^{(secondary)}(\vec{v}_s,\vec{x}_s,t_s) = 0$ by selecting the initial point of the secondary cloud phase space trajectory $(\vec{v}_s,\vec{x}_s,t_s)$ at a point on the primary cloud phase space trajectory where the secondary cloud distribution originates and is hence zero by definition.

In this paper, a general model for the primary cloud atoms (or molecules) is explicitly developed and will include expressions to calculate the relevant plasma input rates supplied to the plasma torus by the primary cloud. A model for the secondary cloud atoms (or molecules) is also given but is more briefly outlined. For simplicity, the general model developed will adopt the language appropriate to a gas cloud of atoms but, with slight generalization, will equally well apply to a molecular gas cloud. For a gas cloud of atoms, the primary cloud population is much brighter than the secondary cloud population

in the general vicinity of Io's orbit, but the secondary cloud population extends throughout and beyond the planetary magnetosphere and provides a background density and cloud brightness into which the primary cloud population merges.

Physics of an Ensemble Packet

A neutral gas cloud of Io may be described for the primary atom population discussed above by following the space-time history of neutral atoms ejected from the surface of the satellite (in low atmospheric density limit) or from the exosphere of the satellite (in the presence of a substantial atmosphere). Without loss of generality, a spherical exobase of radius R_E centered on Io is adopted. For a differential surface area element $d\Omega \left(= R_E^2 \sin\Phi \, d\Phi d\Theta \right)$ of the exobase centered on the angular direction $\hat{\Omega} = (\Theta,\Phi)$, let the neutral flux (number of atoms ejected per unit area, per unit initial velocity interval, per unit time) in the initial velocity interval $\vec{\omega}$ to $\vec{\omega} + d\vec{\omega}$ and at the absolute time t_b be denoted by $\phi(\vec{\omega},\hat{\Omega},t_b)$. The rate at which these atoms are ejected from the surface element is then

$$\phi(\vec{\omega}, \hat{\Omega}, t_b) \, d\Omega \, d\vec{\omega}. \tag{11.a}$$

In terms of the one-particle distribution function of the preceeding subsection, the flux ϕ is defined by

$$\phi(\vec{\omega}, \hat{\Omega}, t_b) = \vec{\omega} \cdot \hat{\Omega} \, f^{(\text{primary})}(\vec{\omega}, \vec{x}_b, t_b) \tag{11.b}$$

where $\vec{x}_b = (R_E, \Theta, \Phi)$ is the spherical polar coordinate location of the surface area element $d\Omega$.

To describe the neutral cloud and its impact on the planetary magnetosphere, it is sufficient to follow in time an ensemble packet of atoms for each neutral species initially ejected in an absolute time interval t_b to $t_b + dt'$, where t' is defined at the flight time since the packet was initially ejected from the exobase at time t_b. For one such neutral species, the motion of a packet is depicted in Figure 1. A number of physical quantities will be defined for the packet in this section. The complete description of a neutral cloud for a particular physical quantity is obtained by integrating the packet contribution for this quantity over its complete flight time and

over all initial exobase conditions. To develop this description, the location of the center of the packet at flight time t' may be denoted by $\vec{r}(t', |\vec{\omega}, \hat{\Omega})$ in a coordinate system fixed relative to the satellite. In the case of a sodium or potassium cloud, the additional force of solar radiation pressure experienced by the packet atoms as they resonantly scatter sunlight requires a more complex solution for the packet location (see Smyth 1979, 1983) that depends in addition on the present value of the absolute time, $t_b + t'$, and hence must be denoted by $\vec{r}(t', t_b | \vec{\omega}, \hat{\Omega})$. This absolute time dependence is introduced because the magnitude of the solar radiation force is modulated by the doppler motion that occurs between the sun and the packet atoms in the satellite frame as Io executes circular motion about Jupiter and as Jupiter moves on its elliptical orbit about the sun.

As an ensemble packet of atoms moves through the circumplanetary space, it may experience ionization, charge exchange, excitation, and even elastic collisions because of its interactions with the Io plasma torus. Neutral-neutral collisions are generally not important (except for recapture near Io and Jupiter where they are easily included) because the accumulated column density determined by the relatively short lifetime of cloud atoms is small. Electron impact ionization, photoionization, and charge exchange reactions remove atoms from the packet and hence determine its decay lifetime. Ionization processes also supply new ions to the planetary magnetosphere. Charge exchange processes modify the ion composition and energy of the Io plasma torus and also provide a flux of high-speed neutrals that (unless captured in the middle magnetosphere) escape from the planetary system. Electron impact excitation processes for neutral oxygen and sulfur atoms provide a photon emission mechanism for these two neutral gas clouds. Elastic ion-neutral collisions alter the trajectory of atoms in the packet and, if important, require that this momentum transfer information be properly incorporated in determining $\vec{r}(t', t_b | \vec{\omega}, \hat{\Omega})$ for the secondary atom population as described in the previous subsection.

To describe the interactions of the ensemble packet of atoms with the plasma torus, it is necessary at an absolute time t to map a location $\vec{R}$ in the satellite fixed coordinate system where the packet location $\vec{r}(t', t_b | \vec{\omega}, \hat{\Omega})$ is specified to a location $\vec{\vec{R}}$ in the magnetic (or, more correctly and generally, what shall be called the plasma) coordinate frame where the plasma properties are specified. The general transformation for this mapping, which is a

function of the absolute time t, will be denoted as follows:

$$\vec{\vec{R}} = \vec{\vec{T}}(t) \cdot \vec{R} + \vec{D}(t) \quad . \tag{12}$$

The tensor part of the transformation, $\vec{\vec{T}}(t)$, includes the relative rotational motion and the tilt angle between the satellite coordinate frame and the plasma torus coordinate frame. The vector part of the transformation, $\vec{D}(t)$, includes the more complex mapping required between the satellite frame and the plasma frame for a dipole offset of the origin of the magnetic and planetary spin coordinate frames as well as for the additional shift of the center of the plasma torus produced by an east-west electric field such as proposed by Barbosa and Kivelson (1983) and Ip and Goertz (1983). The location of a packet at flight time t' in the plasma coordinate system is then given as follows:

$$\vec{\vec{r}}(t',t_b|\vec{\omega},\hat{\Omega}) = \vec{\vec{T}}(t_b + t') \cdot \vec{r}(t',t_b|\vec{\omega},\hat{\Omega}) + \vec{D}(t_b+t') \quad . \tag{13}$$

The velocity of the packet $\vec{\vec{v}}(t',t_b|\vec{\omega},\hat{\Omega})$ at flight time t' in the plasma coordinate system is then determined directly by time differentiation of (13).

In the remainder of this subsection, the ensemble packet contributions for a number of neutral cloud physical quantities of interest (e.g. density, photon emission rate, neutral loss rate, and various plasma input rates to the magnetosphere) are formulated. To facilitate this formulation, a hat "$\hat{}$" notation is adopted to indicate that a physical quantity is described in terms of its phase space representation $(t',t_b|\vec{\omega},\hat{\Omega})$ along its phase space trajectory. Thus, for a general physical quantity Q, its ensemble packet contribution will be denoted by $\hat{Q} = \hat{Q}(t',t_b|\vec{\omega},\hat{\Omega})$. For an observer in a coordinate frame $(\vec{r}_0,t_0)$, the space/time description of the physical quantity $Q(\vec{r}_0,t_0)$ is then determined, as discussed in a later section, from $\hat{Q}$ by evaluating its ensemble average $\langle\hat{Q}\rangle$.

The number of atoms in an ensemble packet at flight time t' depend upon the loss processes suffered by the packet since its beginning at time t_b. For an ensemble packet at a location $\vec{\vec{r}}$ having a velocity $\vec{\vec{v}}$ in the plasma coordinate frame, the lifetime of cloud atoms is denoted by $\tau(\vec{\vec{r}},\vec{\vec{v}})$. The velocity dependence is required in the lifetime to calculate properly the cloud atom charge exchange reaction rates with the plasma torus ions. The

loss collision frequency for the packet is then given by

$$\hat{\nu}(t',t_b|\vec{\omega},\hat{\Omega}) = [\tau(\vec{\tilde{r}}(t',t_b|\vec{\omega},\hat{\Omega}),\vec{\tilde{v}}(t',t_b|\vec{\omega},\hat{\Omega}))]^{-1} \tag{14}$$

and the probability that the ensemble packet of atoms at flight time t' exists is defined as follows:

$$\mathbf{P}(t',t_b|\vec{\omega},\hat{\Omega}) = \exp\left[-\int_0^{t'} \hat{\nu}(t'',t_b|\vec{\omega},\hat{\Omega})\, dt''\right] . \tag{15}$$

The number of atoms in the packet at flight time t' is then given by

$$\hat{n}\,(t',t_b|\vec{\omega},\hat{\Omega})\, d\Omega\, d\vec{\omega}\, dt' \tag{16}$$

where

$$\hat{n}\,(t',t_b|\vec{\omega},\hat{\Omega}) = \mathbf{P}\,(t',t_b|\vec{\omega},\hat{\Omega})\phi(\vec{\omega},\hat{\Omega},t_b) \tag{17}$$

is the number of atoms per unit surface element $d\Omega$ at the initial surface location $\hat{\Omega}$, per unit initial velocity volume $d\vec{\omega}$ at the initial velocity $\vec{\omega}$, and per unit time interval dt' at the flight time t'.

The number of photons emitted by an ensemble packet at flight time t' depends upon its photon excitation mechanism. The two important mechanisms, electron impact excitation in the plasma torus and solar resonance scattering, are described by an atom excitation rate (i.e. photons per atom per unit time) denoted by $J_\lambda(\vec{\tilde{r}}, v_s)$ for an emission line with wavelength λ. The position vector $\vec{\tilde{r}}$ of the packet in the plasma coordinate frame is required in calculating the electrom impact excitation rate for oxygen and sulfur atoms. The radial speed v_s of the packet relative to the sun is required in calculating the solar resonance scattering excitation rate for sodium, potasium, oxygen and sulfur. The photon emission rate (i.e. number of photons emitted per unit time) at wavelength λ for the packet at flight time t' is then given by

$$\hat{I}_\lambda(t',t_b|\vec{\omega},\hat{\Omega})\, d\Omega\, d\vec{\omega}\, dt' \tag{18}$$

where

$$\hat{I}_\lambda(t',t_b|\vec{\omega},\hat{\Omega}) = J_\lambda\left(\vec{r}(t',t_b|\vec{\omega},\hat{\Omega}),\ v_s(t',t_b|\vec{\omega},\hat{\Omega})\right)\ \hat{n}(t',t_b|\vec{\omega},\hat{\Omega})\ . \qquad (19)$$

The rate at which neutral atoms are lost from the packet at flight time t' is determined from the time derivative of (17) and is given by

$$\mathbf{P}\left(\frac{\partial \quad (t',t_b|\vec{\omega},\hat{\Omega})}{\partial t'}\right)\ \phi(\vec{\omega},\hat{\Omega},t_b)\ d\Omega\ d\vec{\omega}\ dt' \qquad (20)$$

which may be written in terms of a loss rate

$$\hat{L}(t',t_b|\vec{\omega},\hat{\Omega})\ d\Omega\ d\vec{\omega}\ dt' \qquad (21)$$

where

$$\hat{L}(t',t_b|\vec{\omega},\hat{\Omega}) = \hat{\nu}(t',t_b|\vec{\omega},\hat{\Omega})\ \hat{n}(t',t_b|\vec{\omega},\hat{\Omega})\ . \qquad (22)$$

Loss processes contributing to the collision frequency $\hat{\nu}$ in (22) occur for the first four types of neutral reactions summarized in Table 3, where the neutral cloud atoms are denoted by the general chemical symbol Y. (It should be noted in passing that to generalize the collision frequency $\hat{\nu}$ for molecular gas clouds, dissociative reactions would from this point forward have to be properly included.) It should be emphasized that the expression (21) is <u>not</u>, however, the <u>net</u> rate at which ions are deposited into the magnetosphere by the packet, since charge exchange reactions of type C in Table 3, while providing from the packet a new ion (Y^+), simultaneously remove an old ion (X^+) from the magnetosphere by production of a fast escaping neutral.

In general, to determine the impact of the neutral cloud on the magnetosphere it is necessary to simultaneously assess the contributions of the packets of several neutral clouds on the plasma torus because of reactions of type C in Table 3. It is of interest to determine these contributions not only for the net ion loading rate $\dot{N}$ but also for the plasma mass loading rate $\dot{M}$, and for the ion energy input rate $\dot{E}$. For a mixture of N neutral gas species (j=1,2,...,N), the instantaneous packet contributions to any one of these three input rates can be formulated (see Smyth and Shemansky 1983) and will be denoted by $\hat{\dot{R}}(t',t_b|\vec{\omega},\hat{\Omega})$, where

$$\hat{R} = \sum_{j=1}^{N} [\hat{\xi}_j \hat{L}_j - \hat{\eta}_j \hat{P}_j] \ . \tag{23}$$

Here $\hat{L}_j$ is the loss rate of the packet for the j-species defined in a parallel manner to (22), and $\hat{P}_j$ is the production rate of the packet for the j-species as determined from the reactions of type C in Table 3. For the three cases of interest, $\hat{\xi}_j$ and $\hat{\eta}_j$ are defined in Table 4, where V_R is the relative velocity between the neutral atom Y and the plasma coordinate frame at the time the neutral is lost from the packet, and V_T is the thermal energy of the X^+ ion at the time it is converted to a fast neutral because of reactions of type C in Table 3.

Combining the ionization reactions A and B in Table 3 into a single term, the collision frequency $\hat{\nu}_j(t', t_b|\vec{\omega}, \hat{\Omega})$ for the j species may be divided into a contribution from ionization (I), charge exchange (CE), and charge transfer (CT) as follows:

$$\hat{\nu}_j = \hat{\nu}_j^{(I)} + \hat{\nu}_j^{(CE)} + \hat{\nu}_j^{(CT)} \tag{24}$$

The charge exchange collision frequency may be further divided into terms

$$\hat{\nu}_j^{(CE)}(t', t_b|\vec{\omega}, \hat{\Omega}) = \sum_{k=1}^{N} \hat{S}_j^{(k)}(t', t_b|\vec{\omega}, \hat{\Omega}) \tag{25}$$

that describe the individual charge exchange reactions. Here $\hat{S}_j^{(k)}$ is the loss rate for the j-species neutral packet because of the charge exchange reaction that produces a fast k-species neutral (i.e. it is the product of the ion density for the ionized k-species times the reaction rate constant for the charge exchange reaction). Symmetric charge exchange (k=j) and nonsymmetric charge exchange (k≠j) are included. The production rate $\hat{P}_j(t', t_b|\vec{\omega}, \hat{\Omega})$ for all fast neutrals of the j species that are produced by <u>all</u> neutral packets is then given by

$$\hat{P}_j = \sum_{k=1}^{N} \hat{S}_k^{(j)} \hat{n}_k \tag{26}$$

so that the expression (23) may be rewritten as the sum of two different terms

$$\hat{R} = \sum_{j=1}^{N} \hat{\xi}_j (\hat{\nu}_j^{(I)} + \hat{\nu}_j^{(CT)}) \hat{n}_j + \sum_{j=1}^{N} \sum_{k=1}^{N} (\hat{\xi}_j \hat{S}_j^{(k)} \hat{n}_j - \hat{\eta}_j \hat{S}_k^{(j)} \hat{n}_k) \ . \tag{27}$$

The contribution of the charge exchange reactions to (27) is given by the second term. This second term is zero for $\hat{\dot{N}}$, nonzero for $\hat{\dot{M}}$ because of the nonsymmetric reactions, and nonzero for $\hat{\dot{E}}$ because of every charge exchange reaction.

In the case of $\hat{\dot{N}}$, the number of neutrals lost from the j-species packet, $\hat{L}_j$, is divided between the net ion loading rate, $\hat{\dot{N}}_j$, and the production of new fast neutrals, $\hat{\nu}_j^{(CE)}\hat{n}_j$, that escape from the system because of reactions of type C (Table 3):

$$\hat{L}_j = \hat{\dot{N}}_j + \hat{\nu}_j^{(CE)}\hat{n}_j \tag{28}$$

as expected on physical grounds. The fraction of $\hat{L}_j$ that contributes to $\hat{\dot{N}}_j$ is time dependent because of the oscillation of the plasma torus about the satellite plane and other more complex motions that are contained in the transformation (13). For $\hat{\dot{M}}$ and $\hat{\dot{E}}$, the separate j-species contributions are coupled as described by (27). The overall mass and energy conservation is reflected in (23), where the first term is the contribution to the plasma torus by the neutrals lost from the packets, and the second term is the contribution produced by new neutrals being created by the packet-plasma reactions of type C in Table 3.

The cumulative value of the instantaneous rate $\hat{\dot{R}}$ supplied to the plasma torus in a time period T by all of the neutral species packets, each of which has a current flight time t', may also equally well be formulated. For the absolute time interval from t_0-T to t_0, this cumulative value is given by

$$\left[\int_{t_\ell}^{t'} \hat{\dot{R}}\,(t'',\, t_0-t' \,|\vec{\omega},\hat{\Omega})\, dt''\right] d\Omega\, d\vec{\omega}\, dt' \tag{29}$$

where

$$t_\ell = \begin{cases} 0 & \text{if } t' < T \\ t'-T & \text{if } t' > T \end{cases} . \tag{30}$$

The quantity (29) is useful in that, even though the instantaneous rate $\hat{\dot{R}}$ integrated over all flight time is time dependent, its cumulative value (29) averaged overall flight time t' is not time dependent, <u>if</u> the source and sink

processes for the neutral cloud are periodic with the period T. This will be discussed further in a later section. It should be noted here in passing, however, that in addition to the instantaneous contribution (27) or the cumulative contributions (29) of the neutral packets to $\dot{\hat{N}}$, $\dot{\hat{M}}$ and $\dot{\hat{E}}$, the plasma torus may also contribute directly through reactions of type E, F and G in Table 3. These additional processes are not in the realm of the neutral cloud description and may be treated independently.

Physics of an Ensemble Subpacket

A neutral gas cloud of Io may be described for the secondary atom population by following the space-time history of all neutral atoms produced by the primary atom population. To accomplish this explicitly, the secondary atom population will be described in terms of an ensemble subpacket in an analogous way that the primary atom population is described in terms of an ensemble packet. The relationship between the packet and subpacket are illustrated in Figure 2. For a neutral gas subpacket of the j^{th} species, the number of atoms created with initial velocity $\vec{\xi}$ to $\vec{\xi}+d\vec{\xi}$ along the primary packet trajectory $\vec{r}(t',t_b|\vec{\omega},\hat{\Omega})$ in the time interval t' to t'+dt' is given by

$$\hat{S}_j(t',t_b|\omega,\hat{\Omega},\vec{\xi})\ d\hat{\Omega}\ d\vec{\omega}\ dt'\ d\vec{\xi} \tag{31}$$

where

$$\hat{S}_j(t',t_b|\vec{\omega},\hat{\Omega},\vec{\xi}) = \hat{P}_j(t',t_b|\vec{\omega},\hat{\Omega})\ g_j(\vec{\xi}|\vec{\omega},\hat{\Omega},t',t_b) \tag{32}$$

Here, $g_j(\vec{\xi}|\vec{\omega},\hat{\Omega},t',t_b)$ is the local initial velocity distribution for all secondary atoms created at time t' along this packet trajectory and is normalized to unity

$$\int g_j(\vec{\xi}|\vec{\omega},\hat{\Omega},t',t_b)\ d\xi = 1 \tag{33}$$

and $\hat{P}_j$ is given by (26) for the case of charge exchange creation of fast secondary neutrals. For a secondary population created by elastic ion-atom or dissociative electron-molecule collisions, the expression for $\hat{P}_j$ must be appropriately generalized. The creation rate (32) in the subpacket formalism occupies a parallel position to the flux (11.b) in the packet formalism.

The location of the center of the subpacket, originally created at a flight time t"=0 with an initial velocity $\vec{\xi}$ at the primary location $\vec{r}(t',t_b|\vec{\omega},\hat{\Omega})$ and corresponding to the primary trajectory time t_b+t', will be denoted for $t"\geq 0$ by $\vec{\tilde{r}}(t",\vec{\xi};\ t',t_b|\vec{\omega},\hat{\Omega})$. In the plasma coordinate system, the location of the subpacket at a flight time t" is therefore given by

$$\vec{\tilde{r}}(t",\vec{\xi};t',t_b|\vec{\omega},\hat{\Omega}) = \tilde{T}(t_b+t'+t") \cdot \vec{r}(t",\vec{\xi};\ t',t_b|\vec{\omega},\hat{\Omega}) + D(t_b+t'+t") \qquad (34)$$

in an exactly parallel manner to the packet location (13). The velocity of the subpacket in the plasma coordinate system will be denoted by $\vec{\tilde{v}}(t",\vec{\xi};\ t',t_b|\tilde{\omega},\hat{\Omega})$ and is determined by the t" time derivative of (34).

The ensemble subpacket contributions for different neutral cloud physical quantities of interest can be formulated as in the previous section for the packet ensemble. To facilitate this formulation, a double hat "$\hat{\hat{}}$" notation is adopted to indicate that a physical subpacket quantity is described in terms of its phase space representation $(t",\vec{\xi};\ t',t_b|\vec{\omega},\hat{\Omega})$ along its phase space trajectory. The loss collision frequency for the subpacket of the j^{th} species is given by

$$\hat{\hat{\nu}}_j(t",\vec{\xi};\ t',t_b|\vec{\omega},\hat{\Omega}) = [\tau_j(\vec{\tilde{r}}(t",\vec{\xi};\ t',t_b|\vec{\omega},\hat{\Omega}),\ \vec{\tilde{v}}(t",\vec{\xi};\ t',t_b|\vec{\omega},\hat{\Omega}))\ ]^{-1} \qquad (35)$$

parallel to the packet expression (14) and the probability that the ensemble subpacket of atoms at flight time t" exist is defined by

$$P_j(t',\vec{\xi};\ t',t_b|\vec{\omega},\hat{\Omega}) = \exp\ [-\int_{t'}^{t"} \hat{\hat{\nu}}_j(t"',\vec{\xi};\ t',t_b|\vec{\omega},\hat{\Omega})\ dt"'] \ . \qquad (36)$$

The number of atoms in the subpacket of the j^{th} species at time t" is then given by

$$\hat{\hat{n}}_j(t",\vec{\xi};\ t',t_b|\vec{\omega},\hat{\Omega})\ d\Omega\ d\vec{\omega}\ dt'\ d\vec{\xi}\ dt" \qquad (37)$$

where

$$\hat{\hat{n}}_j(t",\vec{\xi};\ t',t_b|\vec{\omega},\hat{\Omega}) = \hat{S}_j(t',t_b|\vec{\omega},\hat{\Omega},\vec{\xi})\ \ P_j(t",\vec{\xi};\ t',t_b|\vec{\omega},\hat{\Omega}) \ . \qquad (38)$$

In a similar manner to the packet quantities defined in the previous section, the subpacket photon emission rate density $\hat{\hat{I}}_\lambda(t",\vec{\xi};\ t',t_b|\vec{\omega},\hat{\Omega})$, the loss

rate density $\hat{\hat{L}}(t'',\vec{\xi};\ t',t_b|\vec{\omega},\hat{\Omega})$, and the plasma input rate densities $\hat{\hat{R}}(t'',\vec{\xi};\ t',t_b|\vec{\omega},\hat{\Omega})$ may be defined parallel to the expressions (18), (21) and (27), respectively.

Kinetic Theory Distribution Function

The kinetic theory distribution function for the neutral gas cloud of the j^{th} species as noted earlier may be divided into a contribution from the primary and secondary atom populations

$$f_j(\vec{v}_o,\vec{x}_o,t_o) = f_j^{(primary)}(\vec{v}_o,\vec{x}_o,t_o) + f_j^{(secondary)}(\vec{v}_o,\vec{x}_o,t_o) \quad . \tag{39}$$

Here, $\vec{v}_o$ and $\vec{x}_o$ are the velocity and spatial coordinates of phase space for an observation coordinate frame, and t_o is the absolute time in the observation frame. The primary and secondary contributions to (39) can be directly expressed, respectively, in terms of the primary packet density $\hat{n}$ and the secondary subpacket density $\hat{\hat{n}}$ defined in the previous two sections:

$$f_j^{(primary)}(\vec{v}_0,\vec{x}_0,t_0) = \int_{\substack{\text{exobase}\\ \text{space}}} d\Omega \int_{\substack{\text{velocity}\\ \text{space}}} d\vec{\omega} \int_{\substack{\text{flight}\\ \text{time}}} \hat{n}_j(t',t_0-t,|\vec{\omega},\hat{\Omega})\ \delta(\vec{r}_0,\hat{\vec{r}}_j)\ \delta(\vec{v}_0,\hat{\dot{\vec{r}}}_j) \tag{40}$$

$$f_j^{(secondary)}(\vec{x}_0,\vec{v}_0,t_0) = \int_{\substack{\text{exobase}\\ \text{space}}} d\Omega \int_{\substack{\text{velocity}\\ \text{space}}} d\vec{\omega} \int_{\substack{\text{flight}\\ \text{time}}} dt' \int_{\substack{\text{velocity}\\ \text{space}}} d\vec{\xi} \int_{\substack{\text{flight}\\ \text{time}}} dt''\ \hat{\hat{n}}_j(t'',\vec{\xi};\ t',t_0-t'|\vec{\omega},\hat{\Omega})\delta(\vec{r}_0,\hat{\hat{\vec{r}}}_j)\delta(\vec{v}_o,\hat{\hat{\dot{\vec{r}}}}_j) \quad . \tag{41}$$

In (40) and (41), $\hat{\vec{r}}$ and $\hat{\dot{\vec{r}}}$ are abbreviated notations for the ensemble packet spatial location and velocity

$$\hat{\vec{r}} = \vec{r}(t',t_0-t'|\vec{\omega},\hat{\Omega}) \ , \quad \hat{\dot{\vec{r}}} = \left[\frac{d}{dt'}\vec{r}(t',t_b|\vec{\omega},\hat{\Omega})\right]_{t_b=t_0-t'} \tag{42}$$

and $\hat{\hat{\vec{r}}}$ and $\hat{\hat{\dot{\vec{r}}}}$ are abbreviated notations for the ensemble subpacket location and velocity

$$\hat{\hat{\vec{r}}} = \vec{r}(t'',\vec{\xi}\ ;t',t_0-t'|\vec{\omega},\hat{\Omega}) \ , \quad \hat{\hat{\dot{\vec{r}}}} = \frac{d}{dt''}\ [\vec{r}(t'',\vec{\xi}\ ;\ t',t_0-t'|\vec{\omega},\hat{\Omega})] \ . \tag{43}$$

The quantities $\delta(\vec{r}_0,\vec{r}_j)$ and $\delta(\vec{v}_0,\dot{\vec{r}}_j)$, respectively, are the spatial volume

projection operator and the velocity volume projection operator defined as follows:

$$\delta(\vec{r}_0,\vec{r}) = \frac{1}{\Delta^3 r_0} \begin{cases} 1 & \text{if } \vec{r}_0 < \vec{R}_0 < \vec{r}_0 + \Delta\vec{r}_0 \\ 0 & \text{otherwise} \end{cases} \tag{44}$$

$$\delta(\vec{v}_0,\dot{\vec{r}}) = \frac{1}{\Delta^3 v_0} \begin{cases} 1 & \text{if } \vec{v}_0 < \vec{V}_0 < \vec{v}_0 + \Delta\vec{v}_0 \\ 0 & \text{otherwise} \end{cases} . \tag{45}$$

Here $\vec{R}_0$ is the location of the ensemble packet (or subpacket) in the observation coordinate frame defined and mapped by an appropriately defined transformation of the form

$$\vec{R}_0 = T_0(t_0) \cdot \begin{Bmatrix} \hat{\vec{r}} \\ \hat{\hat{\vec{r}}} \end{Bmatrix} + \vec{D}_0(t_0) \tag{46}$$

and $\vec{V}_0 = \dot{\vec{R}}_0$ is the velocity of the ensemble packet (or subpacket) in the observation coordinate frame. In addition, the quantities $\Delta^3 r_0$ and $\Delta^3 v_0$ are, respectively, the spatial and velocity volume elements establishing the volume resolution element in the phase space of the observation coordinate system and correspond to the spatial volume $\Delta\vec{r}_0$ about $\vec{r}_0$ and the velocity volume $\Delta\vec{v}_0$ about $\vec{v}_0$.

Spatial Properties of the Neutral Cloud

The spatial properties of the neutral cloud (e.g., the three-dimensional number density or the two-dimensional brightness of the cloud on the sky plane) as well as the physical ion input rates to the planetary magnetosphere can be determined directly from the kinetic theory distribution function (39) or alternatively from the expressions derived from the ensemble packet and subpacket in the previous sections. In the former case, one multiplies the distribution function by a physical quantity of interest, which may in general be a function of $(\vec{r}_0,\vec{v}_0,t_0)$, and integrates the product over the velocity coordinate space $\vec{v}_0$. In the latter case, one defines an ensemble average for the packet and subpacket physical quantity of interest, producing an identical

result to the former method because of the nature of the spatial and velocity volume projection operators (44) and (45). The ensemble average approach will be explicitly developed below and is the description adopted for the numerical evaluation of the neutral cloud model discussed in the next section.

If an ensemble packet quantity (e.g., $\hat{n}$, $\hat{I}_\lambda$, $\hat{\dot{N}}$) and its subpacket quantity (e.g., $\hat{\hat{n}}$, $\hat{\hat{I}}_\lambda$, $\hat{\hat{\dot{N}}}$) are denoted respectively as $\hat{Q}(t', t_b|\vec{\omega},\hat{\Omega})$ and $\hat{\hat{Q}}(t'', \vec{\xi};\ t', t_b|\vec{\omega},\hat{\Omega})$, and if the corresponding ensemble averaged physical quantity in the observer's coordinate frame at $\vec{r}_0$ and at an absolute time t_0 is denoted by $Q(\vec{r}_0, t_0)$, then

$$Q(\vec{r}_0, t_0) = \langle\hat{Q}\rangle + \langle\hat{\hat{Q}}\rangle \tag{47}$$

where

$$\langle\hat{Q}\rangle = \int_{\text{exobase}} d\Omega \int_{\substack{\text{velocity}\\ \text{space}}} d\vec{\omega} \int_{\substack{\text{flight}\\ \text{time}}}^{\infty} dt'\ \hat{Q}(t', t_0 - t'|\vec{\omega},\hat{\Omega})\,\delta(\vec{r}_0, \hat{\vec{r}}) \tag{48}$$

$$\langle\hat{\hat{Q}}\rangle = \int_{\text{exobase}} d\Omega \int_{\substack{\text{velocity}\\ \text{space}}} d\vec{\omega} \int_{\substack{\text{flight}\\ \text{time}}}^{\infty} dt' \int_{\substack{\text{velocity}\\ \text{space}}} d\vec{\xi} \int_{\substack{\text{flight}\\ \text{time}}} dt''\ \hat{\hat{Q}}(t'', \vec{\xi};\ t', t_0 - t'|\vec{\omega},\hat{\Omega})\,\delta(\vec{r}_0, \hat{\hat{\vec{r}}}) \tag{49}$$

where $\hat{\vec{r}}$ and $\hat{\hat{\vec{r}}}$ are given by (42) and (43) and where the volume projection operator $\delta(\vec{r}_0, \vec{r})$ is defined by (44). To project an ensemble average physical quantity $Q(\vec{r}_0,\ t_0)$ onto the observer's viewing plane, as is appropriate for the gas density to obtain a column density or for the volume photon emission rates to obtain an image of the cloud brightness, an integration along the line of sight in the observer's coordinate frame is required in addition to those specified in (48) and (49). For the simple case of no parallax with the z_0-axis along the line of sight, the column integrated quantity is given by

$$Q(x_0, y_0 t_0) = \int_{-\infty}^{\infty} Q(\vec{r}_0, t_0)\, dz_0. \tag{50}$$

In this manner, the basic properties of the cloud and also its interactions with the magnetosphere may be calculated.

It should be noted that if the ensemble packet quantity and the packet trajectory are periodic with period T in their initial ejection time t_b, that is, if

$$\hat{Q}(t',t+T|\vec{\omega},\hat{\Omega}) = \hat{Q}(t',t|\vec{\omega},\hat{\Omega}) \tag{51a}$$

$$\vec{r}(t',t+T|\vec{\omega},\hat{\Omega}) = \vec{r}(t',t|\vec{\omega},\hat{\Omega}) \ , \tag{51b}$$

it then follows that the corresponding ensemble average physical quantities of the neutral cloud (47), although time dependent in general, are also periodic with the period T

$$Q(\vec{r}_0,t_0 + T) = Q(\vec{r}_0,t_0) \ . \tag{52}$$

In general, the ensemble averaged value of the cumulative value [see (29) and (30)] of any packet quantity $\hat{Q}$ integrated over a time t_0-T to t_0

$$< [\int_{t_\ell}^{t'} \hat{Q}(t'',t_0-t|\vec{\omega},\hat{\Omega}) \, dt''] > \tag{53}$$

is exactly equal to the ensemble average value of the instantaneous packet quantity $\hat{Q}$ integrated over the time interval

$$\int_{t_0-T}^{t_0} <\hat{Q}> \, dt_0' \tag{54}$$

as can be readily verified. A similar result also holds for the subpacket quantity. If (51) holds, the quantities (53) or (54) are also explicitly independent of the time t_0, as would, of course, be expected purely on physical grounds. For $\hat{Q} = \hat{L}$, this time-independence is clearly illustrated in the simple case of a constant flux

$$\phi(\vec{\omega},\hat{\Omega},t_b) = \phi(\vec{\omega},\hat{\Omega}) \tag{55}$$

by the obvious result

$$\int_{\substack{\text{all}\\\text{space}}} d\vec{r}_0 \int_{t_0}^{t_0+T} <\hat{L}> \, dt_0' = T \int_{\text{exobase}} d\Omega \int_{\substack{\text{velocity}\\\text{space}}} d\vec{\omega} \, \phi(\vec{\omega},\hat{\Omega}) \tag{56}$$

developed directly from (20) and (48).

The general periodic relationship (52) and the equality of (53) and (54) are useful in studying the impact of the neutral clouds on the magnetosphere. A period T of approximately 13 hours exists between Io and its location in the oscillating/rotating magnetosphere if east-west torus differences are assumed small or zero. If on the other hand, east-west torus differences cannot be ignored, a period T of approximately 32 days exists for recurrence of the same east-west position and System III magnetic longitude of Io. To illustrate the impact of the the neutral clouds, the packet expression (28) is summed over the various neutral cloud species and its ensemble average is taken to obtain

$$\langle \hat{L} \rangle = \langle \hat{\dot{N}} \rangle + \langle \sum_{j=1}^{N} \hat{\nu}_j^{(CE)} \hat{n}_j \rangle \ . \tag{57}$$

This expression divides the instantaneous total packet neutral loss rate of the cloud $\langle \hat{L} \rangle$ into its instantaneous net ion loading rate for the magnetosphere $\langle \hat{\dot{N}} \rangle$ and its instantaneous production rate of fast neutrals $\langle \sum_j \hat{\nu}_j^{(CE)} \hat{n}_j \rangle$. This partitioning is time as well as spatially dependent. The latter term of (57) is, of course, the rate at which subpacket fast neutrals are produced. If the packet periodicity (51) holds, the period averaged value of each term in (57) is independent of time, so that the average fractions of neutrals contributing to the net ion loading rate and to the production of fast neutrals are given, respectively, by

$$f^{(\dot{N})}(\vec{r}_o) = \overline{\langle \sum_{j=1}^{N} (\hat{\nu}_j^{(I)} + \hat{\nu}_j^{(CT)}) \hat{n}_j \rangle} \ / \ \overline{\langle \sum_{j=1}^{N} \hat{\nu}_j \hat{n}_j \rangle} \tag{58a}$$

and

$$f^{(fast)}(\vec{r}_o) = \overline{\langle \sum_{j=1}^{N} \hat{\nu}_j^{(CE)} \hat{n}_j \rangle} \ / \ \overline{\langle \sum_{j=1}^{N} \hat{\nu}_j \hat{n}_j \rangle} \tag{58b}$$

where the brackets "<>" denote the packet ensemble average and the bar indicates periodic accumulation, that is

$$\overline{\langle \hat{Q} \rangle} = \int_{t_o}^{t_o+T} \langle \hat{Q} \rangle \, dt'_o = \int_{t_o}^{t_o+T} Q(\vec{r}_o, t'_o) \, dt'_o \tag{58c}$$

and where by construction

$$f^{(\dot{N})}(\vec{r}_o) + f^{(fast)}(\vec{r}_o) = 1 \ . \tag{58d}$$

4. Numerical Approach

The ensemble average of a packet and subpacket quantity given by (47) - (49) and its column integrated value given by (50) may be evaluated numerically. For the packet description, this is accomplished by dividing the exobase into many small area elements. On each area element, the initial velocity distribution as well as the absolute flux are specified independently. For each initial condition specified on an area element, a trajectory $\vec{r}(t',t_b|\vec{\omega},\hat{\Omega})$ for an ensemble packet is calculated for sufficiently long flight time t' to determine accurately the cloud properties. Along each trajectory, the packet quantities $\hat{Q}$ of interest are calculated and accumulated in their appropriate spatial volume (or area of the sky plane) in such a way to determine the packet ensemble average (48) or its contribution to the column-integrated ensemble average (50). For the subpacket description, the source density rate $\hat{S}$ for the subpacket as defined by (31) is calculated in the packet description along the packet trajectory and has the analogous role that the flux (11a) has in the packet description. The source density rate $\hat{S}$ is numerically divided into many small packet flight time increments along the packet trajectory and from each increment the subpacket trajectories $\vec{r}(t'',\vec{\xi};\ t',t_b|\vec{\omega},\hat{\Omega})$ are calculated for sufficiently long flight time t'' to determine accurately the cloud properties. Along each trajectory, the subpacket quantities $\hat{\hat{Q}}$ of interest are calculated and accumulated in the appropriate spatial volume element of the observation coordinate frame.

The packet trajectories $\vec{r}(t',t_b|\vec{\omega},\hat{\Omega})$ and subpacket trajectories $\vec{r}(t'',\vec{\xi};\ t',t_b|\vec{\omega},\hat{\Omega})$ may be determined by solving the standard (Smyth and McElroy 1977) or modified (Smyth 1983) circular-restricted three-body equations of motion for each prescribed initial condition. The modified equations are required for the sodium and potassium cloud because of the additional effects of solar radiation pressure (Smyth 1979, 1983) on these atoms. The equations of motion are solved numerically by applying a straightforward Runge Kutta technique. The time steps employed in the numerical solution must be selected small enough not only to determine an accurate trajectory but also to insure that the space and time resolution of the ensemble average quantities (47), which are quite sensitive to the oscillational/rotational motion of the plasma torus, are calculated to the level of desired accuracy.

For a particular neutral cloud, calculation of the packet quantity $\hat{Q}$, the subpacket quantity $\hat{\hat{Q}}$ and their ensemble averages (48) and (49) requires firstly that the relevant reactions and their rates (symbolically indicated by A-E in Table 3) and also the excitation rates (18) be identified and defined, and secondly that the space/time properties of the plasma torus be specified along the packet and subpacket trajectories. For the sodium cloud, this information is presented in the companion paper (Smyth and Combi 1986) in this issue.

5. Summary

A brief review of Io's local atmosphere and its extended gas clouds as well as their interactions with the planetary magnetosphere was given in section 2. The Io neutral clouds were seen to occupy a central position in understanding the coupled planet-satellite-magnetosphere system. Analysis of earth-based, rocket, or earth-orbiting satellite observations of neutral cloud emissions provides a direct, very promising, and still largely untapped approach for increasing our knowlege and understanding of complex physical phenomena in the system. Physical realistic models for the neutral clouds are essential in this analysis. These models must include the complex space-time interactions that occur between the neutral clouds and the plasma torus which have hitherto not been incorporated. The general Io neutral cloud model developed here includes these interactions and provides a general and solid base for future analysis of cloud data.

A mathematical description for the general neutral cloud model was presented for Io in section 3. For a given neutral gas species, the description is divided into a primary cloud population that is initially ejected from the satellite exobase and a secondary cloud population that is created in a spatially extended volume by the primary cloud population through various time-dependent processes. For simplicity, the mathematical description for the primary and secondary gas populations are explicitly developed for an atomic cloud, although they may be readily generalized for a molecular cloud. The description of the primary gas cloud may be fundamentally reduced to describing the time evolution of an ensemble packet of gas along its phase space trajectory. The description of the secondary gas cloud may likewise be reduced to describing the time evolution of an ensemble subpacket along its phase space trajectory. The physics of an ensemble packet and ensemble subpacket are presented and are also directly related to the kinetic theory distribution function for the gas cloud. The spatial properties of the neutral cloud as well as various ion input rates to the planetary magnetosphere are obtained from their ensemble packet and subpacket values by evaluating their ensemble averages. A straightforward numerical approach for evaluating the model is outlined with appropriate references that define and present a method of solution for the equations of motion of the phase space trajectories for the ensemble packet and subpacket.

As noted earlier, the general model is applied to the Io sodium cloud in a companion paper (Smyth and Combi 1986) in this issue. The application of the general model to other neutral gas clouds of Io (e.g., K, O, S, SO_2, etc.) will be considered in a series of future papers.

ACKNOWLEDGMENTS

This research was supported by the Planetary Atmospheres Program of the National Aeronautics and Space Administration under grants NASW-3949, NASW-3503, NASW-3387 and NASW-3174. Acknowledgment is also made to the National Center for Atmospheric Research, which is sponsored by the National Science Foundation, for computational time used in implementing the model numerically. W. H. Smyth wishes to thank A. Ezzeddine and K. Burleson for their computational support in the earlier phases of developing this model.

Table 1

Io's Neutral Gas Clouds

Neutral Cloud	First Detection		Cloud Emission		
	Date	Observer	Wavelength (Å)	Intensity (Rayleighs)	Excitation Mechanism
Sodium	1972	R.A. Brown (1974)	5890, 5896	$10^3 - 10^4$	Solar Resonance Scattering
Potassium	1975	L.M. Trafton (1975) J.T. Trauger et al. (1976)	7665, 7699	15 - 300	Solar Resonance Scattering
Oxygen	1980	R.A. Brown (1981)	6300	~ 8	Electron Impact
Sulfur	1981	S.T. Durrance et al. (1983)	1304, 1425	~ 3	Electron Impact

Table 2

Some Studies for Exospheric Problems in Planetary Science

Subject	Reference
1. Cometary Atmospheres	Eddington 1910; Haser 1957, 1966; Keller 1973; Keller and Thomas 1975; Keller and Meier 1976; Combi and Delsemme 1980; Combi 1980; Festou 1981a,b; Combi and Smyth 1985; Combi, Stewart and Smyth 1986
2. Planetary Atmospheres	
• Mercury	Hartle 1971; Hartle, Ogilvie and Wu 1973; Hodges 1974; Hartle, Curtis and Thomas 1975; Smith et al. 1978; Curtis and Hartle 1978; Hodges 1980; Ip 1986; Smyth 1986
• Venus	Penner 1977; Hodges and Tinsley 1981, 1982; Rodriguez, Prather and McElroy 1984; Hodges and Tinsley 1986
• Earth	Chamberlain 1963; Hartle 1973; Bertaux and Blamont 1973; Fahr and Paul 1976; Penner 1977; Hodges, Rohrbaugh and Tinsley 1981; Rodriguez 1983; Bishop 1985
3. Satellite Atmospheres	
• Moon	Hodges 1973; Hartle and Thomas 1974; Hodges 1980
• Titan	Fang, Smyth and McElroy 1976; Smyth and McElroy 1977; Smyth 1981; Shemansky, Smith, Smyth and Combi 1984; Hilton and Hunten 1985; Ip 1985
• Io	Carlson, Matson and Johnson 1975; Fang, Smyth and McElroy 1976; Smyth and McElroy 1977, 1978; Matson et al. 1978; Carlson et al. 1978; Smyth 1979; Goldberg et al. 1980; Macy and Trafton 1980; Smyth 1983; Sieveka 1983; Pilcher et al. 1984; Smyth and Combi 1983, 1984, 1985; Sieveka and Johnson 1985; McGrath and Johnson 1986

Table 3

Classification of Reactions Involving Neutral Species

Neutral-Solar Reactions:

A.	Ionization	$Y + h\nu \rightarrow Y^+ + e$

Neutral-Plasma Reactions:

B.	Ionization	$Y + e \rightarrow Y^+ + 2e$
C.	Charge Exchange	$Y + X^+ \rightarrow Y^+ + X$
D.	Forward Charge Transfer	$Y + X^{++} \rightarrow Y^+ + X^+$

Plasma-Plasma Reactions:

E.	Recombination	$Y^+ + e \rightarrow Y$
F.	Reverse Charge Transfer	$Y^+ + X^+ \rightarrow Y + X^{++}$
G.	Dissociative Recombination	$XY^+ + e \rightarrow X + Y$

Table 4

Definition of the Parameters $\hat{\xi}_j$ and $\hat{\eta}_j$

$\dot{\hat{R}}$	ξ_j	η_j
$\dot{\hat{N}}$	1	1
$\dot{\hat{M}}$	m_j	m_j
$\dot{\hat{E}}$	$\frac{m_j}{2} V_R^2$	$\frac{m_j}{2} V_T^2$

REFERENCES

Bagenal, F. (1985) Plasma Conditions Inside Io's Orbit: Voyager Measurements. J. Geophys. Res., 90, 311.

Bagenal, F. and Sullivan, J.D. (1981) Direct Plasma Measurements in the Io Torus and Inner Magnetosphere of Jupiter. J. Geophys. Res., 86, 8447.

Barbosa, D.D. and Kivelson, M.G. (1983) Dawn-Dusk Electric Field Asymmetry of the Io Plasma Torus. Geophys. Res. Lett., 10, 210.

Bertaux, J. L. and Blamont, J. E. (1973) Interpretation of OGO 5 Lyman Alpha Measurements in the Upper Geocorona. J. Geophys. Res., 78, 80.

Bigg, E.K. (1964) Influence of the Satellite Io on Jupiter's Decametric Emission. Nature 203, 1008.

Binder, A.B., and Cruikshank, D.P. (1964) Evidence of an Atmosphere on Io. Icarus, 3, 299.

Bishop, J. (1985) Geocoronal Structure: The Effects of Solar Radiation Pressure and the Plasmasphere Interaction. J. Geophys. Res., 96, 5235.

Brown, R.A. (1974) Optical Line Emission from Io, in Exploration of the Planetary System: Proceedings, I.A.U. symposium No. 65, Torun, Poland, 5-8 September 1973. (Eds. Woszczyk and Iwaniszewska). D. Reidel Publishing Co., Dordrecht, Boston, pp. 527-531.

Brown, R. A. (1981) The Jupiter Hot Plasma Torus: Observed Electron Temperature and Energy Flow. Ap. J., 244, 1072.

Brown, R.A., Pilcher, C.B. and Strobel, D.F. (1983) Spectrophotometric Studies of the Io Torus, in Physics of the Jovian Magnetosphere (Ed. A.J. Dessler), Cambridge University Press, New York, NY, pp.197-225.

Brown, R.A., and Yung, Y.L. (1976) Io, Its Atmosphere and Optical Emission, in Jupiter, Studies of the Interior, Atmosphere, Magnetosphere, and Satellites (Ed. Gehrels), The University of Arizona Press, Tucson, AZ, pp.1102-1145.

Carlson, R. W., Matson, D. L. and Johnson, T. V. (1975) Electron Impact Ionization of Io's Sodium Emission Cloud. Geophys. Res. Lett., 2, 469.

Carlson, R. W., Matson, D. L., Johnson, T. V. and Bergstralh, J. T. (1978) Sodium D-Line Emission From Io: Comparison of Observed and Theoretical Line Profiles. Astrophys. J., 223, 1082.

Chamberlain, J. W. (1963) Planetary Coronae and Atmospheric Evaporation. Planet. Space Sci., 11, 901.

Cheng, A.F. (1984) Escape of Sulfur and Oxygen from Io. J. Geophys. Res., 89, 3939.

Cloutier, P.A., Daniell, R.E., Jr., Dessler, A.J., and Hill, T.W. (1978) A Cometary Ionosphere model for Io. Astrophys. Space Sci., 55, 93.

Combi, M. R. (1980) Neutral Cometary Atmospheres III. Acceleration of Cometary CN by Solar Radiation Pressure. Ap. J., 241, 830.

Combi, M. R. and Delsemme, A. H. (1980) Neutral Cometary Atmospheres I. An Average Random Walk Model for Photodissociation in Comets. Ap. J., 237, 641.

Combi, M. R. and Smyth, W. H. (1985) Particle-Trajectory Models for the Spatial Distributions of Neutral Cometary Gases. BAAS, 17, 724.

Combi, M. R., Stewart, A. J. F., and Smyth, W. H. (1986) Pioneer Venus Lyman-α Observations of Comet P/Giacobini-Zinner and the Life Expectancy of Cometary Hydrogen. Geophys. Res. Lett., 13 385.

Curtis, S. A. and Hartle, R. E. (1978) Mercury's Helium Exosphere After Mariner 10's Third Encounter. J. Geophys. Res., 83, 1551.

Durrance, S. T., Feldman, P.D., and Weaver, H.A. (1983) Rocket Detection of Ultraviolet Emission from Neutral Oxygen and Sulfur in the Io Torus. Ap. J. Lett., 267, L125.

Eddington, A. S. (1910) The Envelopes of Comet Morehouse (1908c) Mon. Not. Roy. Astron. Soc., 70, 442.

Fahr, H.J., and Paul, G. (1976) Exospheric Velocity Distribution Functions and Derived Gas Dynamical Properties. J. Atmos. Terr. Phys., 38, 841.

Fahr, H.J., and Shizgal, B. (1983) Modern Exospheric Theories and their Observational Relevance. Rev. Geophys. and Space Sci., 21, 75.

Fanale, F.P., Banerdt, W.B., Elson, L.S., Johnson, T.V. and Zurek, R.W. (1982) Io's Surface: Its Phase Composition and Influence on Io's Atmosphere and Jupiter's Magnetosphere. in Satellites of Jupiter. (Ed. D. Morrison), University of Arizona Press, Tucson, AZ, pp.756-781.

Fanale, F.P., Johnson, T.V. and Matson, D.L. (1977) Io's Surface and the Histories of the Galilean Satellites. in Planetary Satellites (Ed. Joseph A. Burns), University of Arizona Press, Tucson, AZ, pp.379-405.

Fang, T.-M. Smyth, W. H. and McElroy, M. B. (1976) The Spatial Distribution of Long Lived Gas Clouds Emitted by Satellites in the Outer Solar System. Planet. Space Sci., 24, 577.

Festou, M. C. (1981a) The Density Distribution of Neutral Compounds in Cometary Atmospheres. I. Models and Equations. Astron. Astrophys., 95, 69.

Festou, M. C. (1981b) The Density Distribution of Neutral Compounds in Cometary Atmospheres. II. Production Rate and Lifetime of OH Radicals in Comet Kobayashi-Beger-Milon (1975IX). Astron. Astrophys., 96, 52.

Goldberg, B. A., Mekler, Yu., Carlson, R. W., Johnson, T. V. and Matson, D. L. (1980) Io's Sodium Emission Cloud and the Voyager 1 Encounter. Icarus, 44, 305.

Goldberg, B.A., Garneau, G.W., and LaVoie, S.K. (1984) Io's Sodium Cloud. Science 226, 512.

Haff, P.K., Watson, C.C., and Yung, Y.L. (1981) Sputter Ejection of Matter from Io. J. Geophys. Res., 86, 6933.

Hartle, R. E. (1971) Model for Rotating and Nonuniform Planetary Exospheres. Phys. Fluids, 14, 2592.

Hartle, R. E. (1973) Density and Temperature Distributions in Non-Uniform Rotating Planetary Exospheres with Applications to Earth. Planet. Space Sci., 21, 2123.

Hartle, R. E., Ogilvie, K. W. and Wu, C. S. (1973) Neutral and Ion-Exospheres in the Solar Wind with Applications to Mercury. Planet. Space Sci., 21, 2181.

Hartle, R. E. and Thomas, G. E. (1974) Neutral and Ion Exosphere Models for Lunar Hydrogen and Helium. J. Geophys. Res., 79, 1519.

Hartle, R. E., Curtis, S. A. and Thomas, G. E. (1975) Mercury's Helium Exosphere. J. Geophys. Res., 80, 3689.

Haser, L. (1957) Distribution d'intensite dans la tete d'une comete. Bull. Acad. Roy. Soc. Belgique, 43, 740.

Haser, L. (1966) Nature et Origine des Cometes, 13th Liege Symp., 233.

Hilton, D. A. and Hunten, D. M. (1985) A Partially Collisional Model of the Titan Hydrogen Torus. BAAS, 17, 696.

Hodges, R. R. (1973) Helium and Hydrogen in the Lunar Atmosphere. J. Geophys. Res., 78, 8055.

Hodges, R. R., Jr. (1974) Model Atmospheres for Mercury Based on a Lunar Analogy. J. Geophys. Res., 79, 2881.

Hodges, R. R., Jr. (1980) Methods for Monte Carlo Simulation of the Exospheres of the Moon and Mercury. J. Geophys. Res., 85, 164.

Hodges, R. R. and Tinsley, B. A. (1981) Change Exchange in Venus Ionosphere as the Source of the Hot Exospheric Hydrogen. J. Geophy. Res., 86, 7649-7656.

Hodges, R. R. and Tinsley, B. A. (1982) The Influence of Thermospheric Winds on Exospheric Hydrogen on Venus. Icarus, 51, 440.

Hodges, R. R., Rohrbaugh, R. P., and Tinsley, B. A. (1981) The Effect of the Charge Exchange Source on the Velocity and 'Temperature' Distributions and Their Anisotropies in the Earth's Exosphere. J. Geophys. Res., 86, 6917.

Hodges, R. R. and Tinsley, B. A. (1986) The Influence of Charge Exchange on the Velocity Distribution of Hydrogen in the Venus Exosphere. (preprint)

Hunten, D.M. (1985) Blowoff of an Atmosphere and Possible Application to Io. Geophys. Res. Lett., 12, 271.

Ip, W.-H. (1982) On Charge Exchange and Knock-On Processes in the Exosphere of Io. Ap. J., 262, 780.

Ip. W.-H. (1985) Titan's Hydrogen Torus. In Proceedings, International Workshop on the Atmospheres of Saturn and Titan, 16-19 Spetember 1985, ESA SP-241.

Ip, W.-H. (1986) The Sodium Exosphere and Magnetosphere of Mercury. Geophys. Res. Lett., 13, 423.

Ip, W.-H. and Goertz, C.K. (1983) An Interpretation of the Dawn-Dusk Asymmetry of UV Emission from the Io Plasma Torus. Nature, 302, 232.

Keller, H. U. (1973) Hydrogen Production Rates of Comet Bennett (1969i) in the First Half of April 1970. Astron. & Astrophys., 27, 51.

Keller, H. U. and Thomas, G. E. (1975) A Cometary Hydrogen Model: Comparison with OGO-5 Measurements of Comet Bennett (1970II). Astron. & Astrophys., 39, 7.

Keller, H. U. and Meier, R. R. (1976) A Cometary Hydrogen Model for Aribitary Observational Geometry. Astron. & Astrophys., 52, 273.

Kliore, A., Cain, D.L., Fjeldbo, G., and Seidel, B.L. (1974) Preliminary Results on the Atmospheres of Io and Jupiter from the Pioneer 10 S-Band Occultation Experiment. Science, 183, 323.

Kumar, S. (1979) The Stability of an SO_2 Atmosphere on Io. Nature, 280, 758.

Kumar, S. (1980) A Model of the SO_2 Atmosphere and Ionosphere of Io. Geophys. Res. Lett., 7, 9.

Kumar, S. (1982) Photochemistry of SO_2 in the Atmosphere of Io and Implications on Atmospheric Escape. J. Geophys. Res., 87, 1677.

Kumar, S. (1984) Sulfur and Oxygen Escape from Io and a Lower Limit to Atmospheric SO_2 at Voyager 1 Encounter. J. Geophys. Res., 89, 7399.

Kumar, S. (1985) The SO_2 Atmosphere and Ionosphere of Io: Ion Chemistry, Atmospheric Escape, and Models Corresponding to the Pioneer 10 Radio Occultation Measurements. Icarus, 61, 101.

Kumar, S. and Hunten, D.M. (1982) The Atmosphere of Io and Other Satellites. in Satellites of Jupiter (Ed. D. Morrison), University of Arizona Press, Tucson, AZ, pp.782-806.

Lanzerotti, L.J. and Brown, W.L. (1983) Supply of SO_2 from the Atmosphere of Io. J. Geophys. Res., 88, 989.

Macy, W.W., Jr., and Trafton, L.M. (1975a) Io's Sodium Emission Cloud. Icarus, 25, 432.

Macy, W., Jr., and Trafton, L. (1975b) A Model for Io's Atmosphere and Sodium Cloud. Ap. J., 200, 510.

Macy, W and Trafton, L. (1980) The Distribution of Sodium in Io's Cloud: Implications. Icarus, 41, 131.

Matson, D. L., Goldberg, B. A., Johnson, T. V. and Carlson, R. W. (1978) Images of Io's Sodium Cloud. Science, 199, 531.

Matson, D.L., Johnson, T.V. and Fanale, F.P. (1974) Sodium D-Line Emission from Io: Sputtering and Resonant Scattering Hypothesis. Ap. J. Lett., 192, L43.

Matson, D.L., and Nash, D.B. (1983) Io's Atmosphere: Pressure Control by Regolith Cold Trapping and Surface Venting. J. Geophys. Res., 88, 4771.

McGrath, M. A., and Johnson, R. E. (1986) Magnetospheric Plasma Sputtering of Io's Atmosphere (preprint).

Morabito, L.A., Synnott, S.P., Kupferman, P.N. and Collins, S.A. (1979) Discovery of Currenty Active Extraterrestrial Volcanism. Science, 204, 972.

Münch, G. and Bergstralh, J.T. (1977) Io: Morphology of its Sodium Emission Region. Pub. A.S.P., 89, 232.

Nash, D.B., Carr, M.H., Gradie, J., Hunten, D.M., and Yoder, C.F. (1986) Io. in Satellites (Ed. J.A. Burns and M.S. Matthews), University of Arizona Press, Tucson, AZ.

Pearl, J., Hanel, R., Kunde, V., Maguire, W., Fox, K., Gupta, S., Ponnamperuma, C., and Raulin, F. (1979) Identification of Gaseous SO_2 and New Upper Limits for Other Gases on Io. Nature, 280, 755.

Penner, J. E. (1977) Photochemistry and Transport Processes for Terrestrial Atmospheric H_2 and Venus Exospheric H. Ph.D. Thesis, Harvard University, Cambridge, Massachusetts

Pilcher, C.B., Smyth, W.H., Combi, M.R., and Fertel, J.H. (1984) Io's Sodium Directional Features: Direct Evidence for a Magnetospheric-Wind-Driven Gas Escape Mechanism. Ap. J., 287, 427.

Pilcher, C.B., and Strobel, D.F. (1982) Emission from Neutrals and Ions in the Jovian Magnetosphere. in Satellites of Jupiter (Ed. D. Morrison), University of Arizona Press, Tucson, AZ, pp.807-845.

Rodriguez, J. M. (1983) Transport Processes in Planetary Atmospheres. Ph.D. Thesis, Dept. of Physics, Harvard University, Cambridge, Massachusetts

Rodriguez, J. M., Prather, M. J. and McElroy, M. B. (1984) Hydrogen on Venus: Exospheric Distribution and Escape. Planet. Space Sci., 32, 1235.

Schneider, N. M., Wells, W. K., Hunten, D. M., and Brown, R. A. (1985) A Novel Method for Measuring Sodium in Io's Bound Atmosphere. BAAS, 17, 699.

Shemansky, D. E. (1984) Private Communication

Shemansky, D. E., Smith, G. R., Smyth, W. H., and Combi, M. R. (1984) The Distribution of Atomic Hydrogen in Saturn's Magnetosphere. BAAS, 16, 712.

Sieveka, E. M. (1983) Charged Particle Erosion of Icy Satellites: Coronal Atmospheres and Surface Redistribution. Ph.D. Thesis, Dept. of Nuclear Engineering and Engineering Physics, University of Virginia.

Sieveka, E.M. and Johnson, R.E. (1984) Ejection of Atoms and Molecules from Io by Plasma-Ion Impact. Ap. J., 287, 418.

Sieveka, E. M. and Johnson, R. E. (1985) Nonisotropic Coronal Atmosphere on IO. J. Geophys. Res., 90, 5327.

Smith, B.A., and Smith, S.A. (1972) Upper Limits for an Atmosphere on Io. Icarus, 17, 218.

Smith, G. R., Shemansky, D. E., Broadfoot, A. L. and Wallace, L. (1978) Monte Carlo Modeling of Exospheric Bodies: Mercury. J. Geophys. Res., 83, 3783.

Smyth, W.H. (1979) Io's Sodium Cloud: Explanation of the East-West Asymmetries. Ap. J., 234, 1148.

Smyth, W. H. (1981) Titan's Hydrogen Torus. Ap. J. 246, 344.

Smyth, W.H. (1983) Io's Sodium Cloud: Explanation of the East-West Assymetries. II. Ap. J., 264, 708.

Smyth, W. H. (1986) The Nature and Variability of Mercury's Sodium Atmosphere. Nature, in press.

Smyth, W. H. and Combi, M. R. (1983) Io's Sodium Cloud: A Model for its Interaction with the Plasma Torus. BAAS, 15, 810.

Smyth, W.H., and Combi, M.R. (1984) Understanding the Escape of Material from Io and its Role in the Planetary Magnetosphere. BAAS, 16, 663.

Smyth, W. H. and Combi, M. R. (1985) Correlating East-West Asymmentries in the Jovian Magnetosphere and the Io Sodium Cloud. BAAS, 17, 695.

Smyth, W.H., and Combi, M.R. (1986) A New Model for Io's Neutral Gas Cloud: Application to the Sodium Cloud. (Companion paper)

Smyth, W.H. and McElroy, M.B. (1977) The Sodium and Hydrogen Gas Clouds of Io. Planet. Space Sci., 25, 415.

Smyth, W. H. and McElroy, M. B. (1978) Io's Sodium Cloud: Comparison of Models and Two-Dimensional Images. Ap. J., 226, 336.

Smyth, W.H. and Shemansky, D.E. (1983) Escape and Ionization of Atomic Oxygen from Io. Ap. J., 271, 865.

Summers, M.E. (1984) Theoretical Studies of Io's Atmosphere. Ph.D. Thesis, Division of Geological and Planetary Sciences, California Institute of Technology.

Summers, M.E., Yung, Y.L. and Haff, P.K. (1983) A Two-Stage Mechanism for the Escape of Na and K from Io. Nature, 304, 710.

Trafton, L. (1975) Detection of a Potassium Cloud near Io. Nature, 258, 690.

Trafton, L. (1980) An Explanation for the Alternating North-South Asymmetry of Io's Sodium Cloud. Icarus, 44, 318.

Trafton, L. (1981) A Survey of Io's Potassium Cloud. Ap. J., 247, 1125.

Trafton, L., and Macy, W., Jr. (1975) An Oscillating Asymmetry of Io's Sodium Emission Cloud. Ap. J. Lett., 202, L155.

Trafton, L., Parkinson, T., and Macy, W. (1974) The Spatial Extent of Sodium Emission around Io. Ap. J. Lett., 190, L85.

Trauger, J.T. (1984) Photometric Images of Sulfur Ions and Sodium Neutrals in the Jupiter/Io Torus. BAAS, 16, 712.

Trauger, J.T. (1985) Doppler-Resolved Spectral Imagery of Io Sodium Phenomena. BAAS, 17, 694.

Trauger, J., Roesler, F. and Münch, G. (1976) Velocity Structure in the Sodium Emission from Io. Bull. AAS, 8, 468.

FIGURE CAPTIONS

Figure 1. Motion of a Neutral Cloud Packet. The mathematical description for the primary population of the neutral cloud based upon the dynamic evolution of neutral cloud packets is depicted. The one neutral cloud packet shown on its trajectory at a flight time $t'>0$ is ejected from a satellite exosphere area element $d\Omega$ with a velocity $\vec{\omega}$ at flight time $t'=0$.

Figure 2. Motion of a Neutral Cloud Subpacket. The mathematical description of the secondary population of the neutral cloud based upon the dynamic evolution of neutral cloud subpackets is depicted. The one neutral cloud subpacket shown on its trajectory at flight time $t">0$ is ejected at flight time $t"=0$ with initial velocity $\vec{\xi}$ from the neutral packet. The location of the neutral packet at the later time ($t">0$) is also indicated.

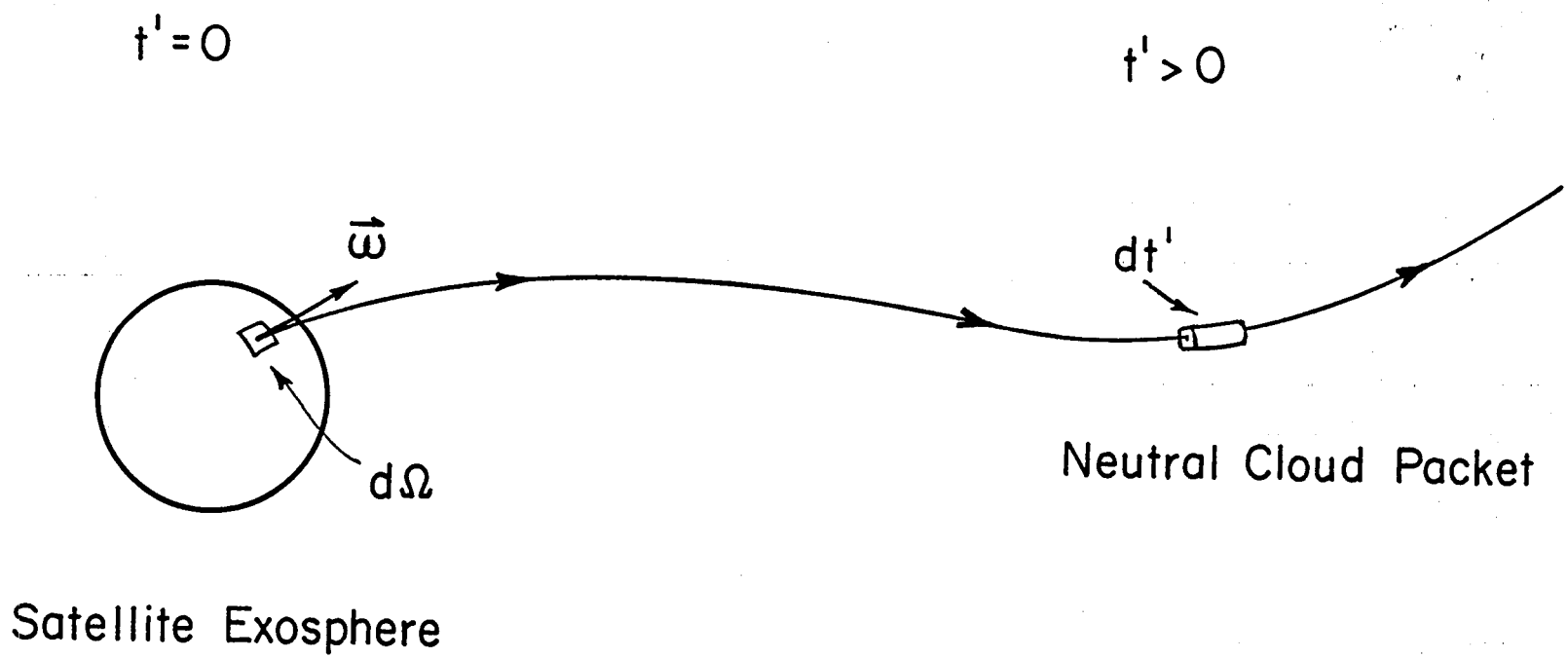
t'=0
t'>0
$\vec{\omega}$
dt'
dΩ
Neutral Cloud Packet
Satellite Exosphere

Figure 1

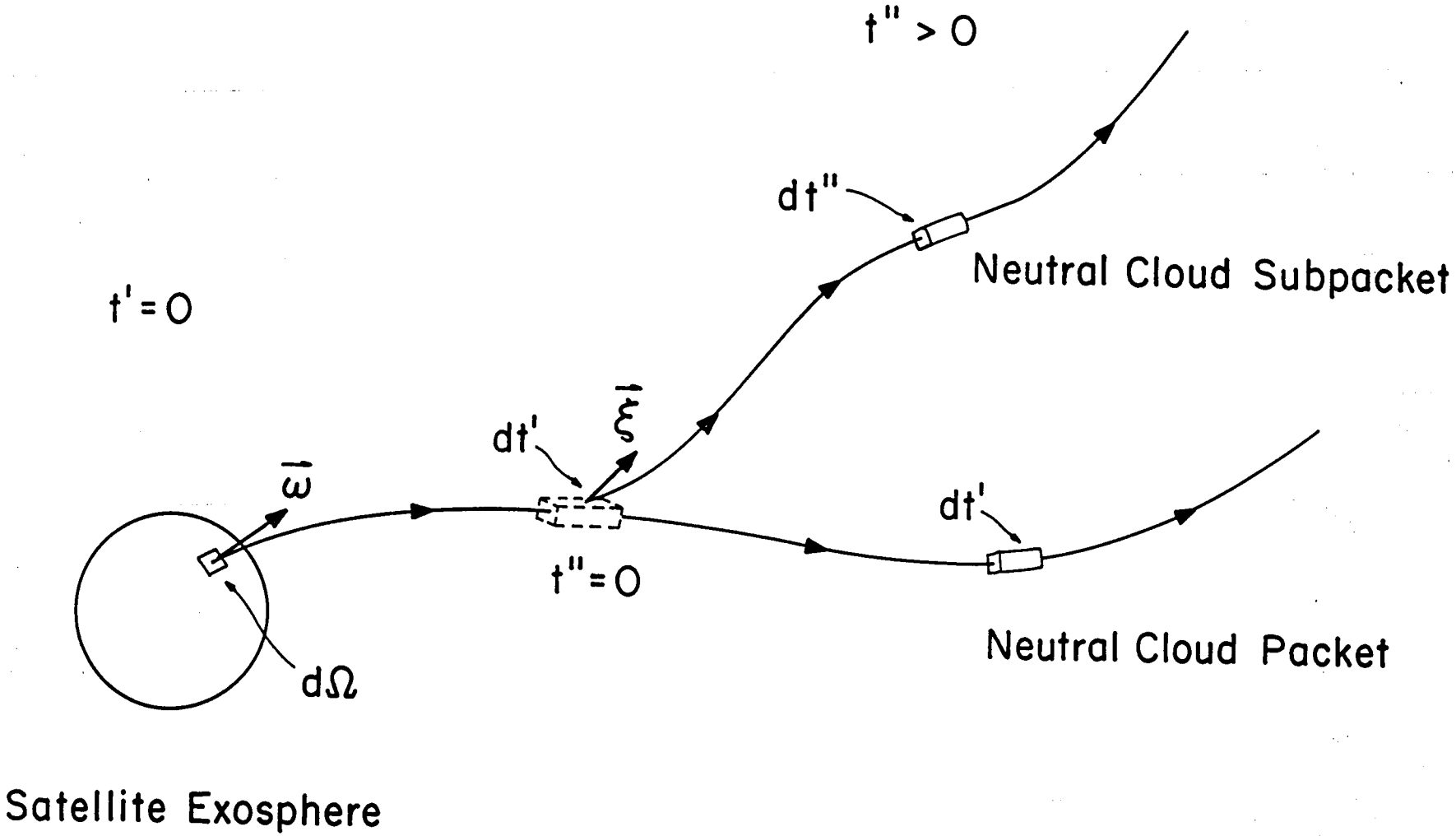
t'' > 0
dt''
Neutral Cloud Subpacket
t' = 0
dt'
$\vec{\xi}$
$\vec{\omega}$
dt'
t'' = 0
Neutral Cloud Packet
dΩ
Satellite Exosphere

Figure 2

Michael R. Combi and William H. Smyth
Atmospheric and Environmental Research, Inc.
840 Memorial Drive
Cambridge, MA 02139-3758